

Phases of theories with fermions in AdS

Astha Kakkar^{a*} and Swarnendu Sarkar^{a,b†}

^a*Department of Physics and Astrophysics, University of Delhi,
Delhi 110007, India*

^b*Department of Physics, Vidyasagar University,
Midnapore 721102, India*

Abstract

We study the phases of Yukawa theories at weak coupling and the Gross-Neveu models in AdS spaces at zero and finite temperature. Following the method used in [15], we first compute the one-loop partition functions, using the generalized eigenfunctions of the Laplacian on Euclidean AdS in the Poincaré coordinates. These functions satisfy desired periodicities under thermal identification. The method replicates results for partition functions known in the literature. We then study the phases of these field theories with fermions as regions in the corresponding parameter spaces at zero temperature. The phases and the corresponding phase boundaries are further identified as a function of the mass-squared of the scalar field and temperature for the Yukawa theories. While for the Gross-Neveu models, the changes in the phases as a function of the fermionic mass and the coupling constant at finite temperature are discussed. The Gross-Neveu-Yukawa model is studied for AdS₄. We also note certain deviations from phases of these theories in flat space.

arXiv:2303.02711v1 [hep-th] 5 Mar 2023

*asthakakkar8@gmail.com

†swarnen@gmail.com

Contents

1	Introduction	2
2	One-loop partition function	5
2.1	Zero temperature: Euclidean AdS_{d+1}	6
2.2	Finite temperature: Thermal AdS_3	8
2.2.1	Thermal AdS_{d+1}	11
3	Study of theories with fermions	14
3.1	Yukawa theory	14
3.1.1	AdS_3	15
3.1.2	AdS_2	17
3.1.3	AdS_4	19
3.2	Gross-Neveu model	22
3.2.1	AdS_3	23
3.2.2	AdS_2	25
3.2.3	AdS_4	27
4	Discussion	29
A	Some details of zero temperature computation	30
A.1	Derivation of the measure $\mu(\lambda)$	30
A.2	λ contour integral in (2.17)	31
A.3	An alternate computation of trace (2.15)	32
B	Effective potentials	34
B.1	Yukawa theory on AdS_4	34
B.2	A different renormalization scheme	36

1 Introduction

Quantum field theories in Anti-de Sitter (AdS) spaces have been studied for quite some time [1]-[10]. In the recent years there has been renewed interest in this area mainly with the aim of obtaining information on non-perturbative flat-space S-Matrix. The idea involves taking flat-space limit, $L \rightarrow \infty$, (L being the AdS length scale) of boundary correlation functions in AdS space. This translates into taking appropriate limits in boundary conformal field theory where newly developed techniques in the conformal field theories can be used. See [11] for a recent status and references therein. Another motivation has been to study the conformal field theories in flat-space with boundaries by considering theories at the critical point in AdS [12]-[14].

Our aim in this paper is however much more modest. We study phases of theories perturbatively in couplings and in $1/N$ (N being the number of flavors) in AdS for a fixed L . The ultraviolet regime

of these theories remains same as that in flat-space but the infrared behavior differs. The results in this case are thus expected to deviate from those of flat-space. An analysis along this line was done in [15] where phases of theories with only scalars at finite temperature was studied after computing effective potentials. Several features which differ from flat space were noted. Symmetry broken phase was found to exist at high temperatures for AdS_3 and AdS_2 . In AdS_2 symmetry breaking was noted in [3] at zero temperature, evading the Coleman-Mermin-Wagner theorem [16, 17]. This was shown to persist at finite temperatures.

In this paper we study the phases of theories with fermions concentrating on the Yukawa theories and the Gross-Neveu models. The essential ingredient utilized in studying these phases is the one-loop partition function for scalars and for fermions. These partition functions have been obtained in the recent past using various methods, see for example [18]-[25]. An alternate method was introduced in [15].

In the initial sections of the paper we derive expressions for fermion one-loop partition function at zero and finite temperatures using the method used in [15] for scalars. The trace (2.5) which is the primary object for our purpose, can be obtained by knowing the degeneracy of the eigenvalues. The spectrum in this case is continuous and ranges between $\pm\infty$. These degeneracies have been worked out quite some time back in [26]. We however take a different route to the computation of the trace. We use the eigenfunctions of the Laplacian operator for Euclidean AdS_{d+1} in Poincaré coordinates which are worked out and studied in [27]-[29]. Though the degeneracy is easily computed, in our method, one does not need to isolate it. The trace then is essentially the Green's function evaluated at coincident points. This method naturally generalizes to the case of thermal AdS_{d+1} .

The finite temperature potentials that we study are obtained by the identification of the Euclidean time in global coordinates, $\tau \rightarrow \tau + \beta$. This can be identified as the quotient space $\mathbb{H}^{d+1}/\mathbb{Z}$. For finite temperature we thus first find the generalized eigenfunctions that are periodic or anti-periodic for bosons and fermions respectively, under the action of the elements of \mathbb{Z} . A similar method has been used for studying field theories on quotient spaces, see for example [30] and for a more recent application for scalars see [31, 32]. It can be shown that the trace obtained using such a method can be re-written in terms of infinite number of images of the Green's functions.

From the analysis of scalars in [15] it was seen that, though the zero temperature contribution to the trace is proportional to the divergent volume of AdS_{d+1} , the finite temperature piece is not. In writing down the effective potential we thus need to regularize this volume. The results of regularized volume which are used in this paper are reviewed in [15]. As mentioned before, the ultraviolet behavior of the theories is same as that of flat space and one needs to implement the usual renormalization. In our setup of the computation of the trace it is natural to use dimensional regularization. The

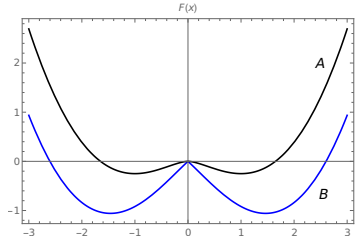


Figure 1: General feature of potentials with cusp for theories with fermions in AdS is shown in blue. The corresponding feature in flat-space is smooth and is shown in black. For illustration we have plotted the function $F(x) = \int_0^x f(y) dy$ vs x . *A*: $f(x) = x \log(|x|)$ and *B*: $f(x) = x \psi^{(0)}(|x|)$.

ultraviolet renormalization then is done by imposing suitable renormalization conditions. A scheme similar to that of the minimal subtraction scheme is also discussed for Yukawa theories in appendix A.3. In the theories with fermions that we study, as compared to flat space effective potential, the **Log**'s are replaced by **PolyGamma** functions with absolute values of arguments. The potentials are thus not smooth and have a cusp. A simple such example is plotted in Figure 1. This feature of the potentials causes a difficulty in the analysis of the phases which are studied numerically.

For Yukawa theories because of the lack of $\phi \rightarrow -\phi$ symmetry the potential is asymmetric about $\phi = 0$. These theories have several parameters which poses an additional complication in the analysis. We first isolate the regions in the parameter spaces at zero temperature corresponding to the number of minima. The phases are then further identified as a function of the scalar mass-squared and temperature. In all the cases we find a phase boundary where two minima exchange dominance at zero temperature. At finite temperature such a transition is found for AdS₂ and AdS₃.

We next study the Gross-Neveu model having $U(N)$ symmetry and four-fermion interaction, originally studied in two dimensions [35]. In flat space the Gross-Neveu model has also been studied extensively in three dimensions. The theory though non-renormalizable perturbatively in the four-fermion coupling constant, has been shown to be renormalizable in the large N expansion [36]. In our analysis we consider this model in AdS₂ and in AdS₃ with tree-level fermion mass m_f . In the large N limit we find that the discrete chiral symmetry that appears in the $m_f = 0$ limit remains broken at zero and at all finite temperatures both for two and three dimensions. This is unlike in flat space where the discrete chiral symmetry is restored beyond a certain temperature [37]-[41]. In four dimensions one needs to include the scalar self interactions for the four-fermion theory to be renormalizable [42]. In the large N limit with proper re-scaling of the parameters by N the potential reduces to that of the Yukawa model in AdS₄.

This paper is organized as follows. We begin section 2 with the basic setup. In section 2.1 we re-

derive a known result for the fermion trace (2.5) for fermions in Euclidean AdS $_{d+1}$. The corresponding expression for thermal AdS $_3$ is computed in section 2.2. This result is then generalized for thermal AdS $_{d+1}$ in section 2.2.1. Section 3 is devoted to the study of phases of theories with fermions. Yukawa theories in various dimensions are analysed in section 3.1. In section 3.2 we study the Gross-Neveu models in two and three dimensions and the Gross-Neveu-Yukawa model in four dimensions. We end the paper with discussions and some future directions in section 4. Some details of computation of the fermion trace (2.5) at zero temperature is given in appendix A. Appendix B.1 contains the expression for potential for AdS $_4$ using renormalized perturbation theory. An alternate renormalization scheme for Yukawa theories is considered in appendix B.2.

2 One-loop partition function

We first highlight the general setup taking the example of Yukawa theory with scalar self-interaction

$$S = - \int d^{d+1}x \sqrt{g} \left[\bar{\psi} (\not{D} + m_f + g\phi) \psi + \frac{1}{2} (\partial_\mu \phi)^2 + V(\phi) \right]. \quad (2.1)$$

The Dirac operator \not{D} is given by

$$\not{D}\psi = \gamma^M D_M \psi = \epsilon_a^M \Gamma^a \left(\partial_M + \frac{1}{8} \omega_M^{bc} [\Gamma_b, \Gamma_c] \right) \psi \quad (2.2)$$

ϵ_a^M is the vielbein and ω_M^{bc} the spin connection. The Euclidean Gamma matrices satisfy $\{\Gamma_b, \Gamma_c\} = 2\delta_{bc}$. Next, writing $\phi = \phi_{cl} + \eta$ and integrating the quadratic action over η and ψ gives the one-loop partition function,

$$\begin{aligned} Z^{(1)} &= \det[\not{D} + M_f(\phi_{cl})] \det[-\square_E + V''(\phi_{cl})]^{-1/2} \exp(-\mathcal{V}_{d+1} V(\phi_{cl})) \\ &= \exp(\text{tr} \log[\not{D} + M_f(\phi_{cl})]) \exp\left(-\frac{1}{2} \text{tr} \log[-\square_E + V''(\phi_{cl})]\right) \exp(-\mathcal{V}_{d+1} V(\phi_{cl})) \end{aligned} \quad (2.3)$$

where $M_f(\phi_{cl}) = m_f + g\phi_{cl}$, \mathcal{V}_{d+1} is the volume of $d+1$ dimensional Euclidean space and $\square_E = \partial_\mu [\sqrt{g} g^{\mu\nu} \partial_\nu] / \sqrt{g}$. The effective potential in terms of the one-loop partition functions for bosons, $Z_b^{(1)}$ and fermions, $Z_f^{(1)}$ is given by,

$$\begin{aligned} V_{eff}(\phi_{cl}) &= -\frac{1}{\mathcal{V}_{d+1}} \log Z_f^{(1)} - \frac{1}{\mathcal{V}_{d+1}} \log Z_b^{(1)} + V(\phi_{cl}) \\ &= -\frac{1}{\mathcal{V}_{d+1}} \text{tr} \log[\not{D} + M_f(\phi_{cl})] + \frac{1}{2\mathcal{V}_{d+1}} \text{tr} \log[-\square_E + V''(\phi_{cl})] + V(\phi_{cl}). \end{aligned} \quad (2.4)$$

The log of the trace can be obtained (up to a constant) by integrating the the following:

$$\frac{1}{2\mathcal{V}_{d+1}}\text{tr}\left[\frac{1}{-\square_E + V''(\phi_{cl})}\right] \quad \text{and} \quad \frac{1}{\mathcal{V}_{d+1}}\text{tr}\left[\frac{1}{\mathcal{D} + M_f(\phi_{cl})}\right]. \quad (2.5)$$

For theories with only scalars the traces were computed and phases were studied in [15]. In the following few sections we compute the trace (2.5) for the fermions at zero and finite temperature. We use the method similar to that of scalars in [15] for computation of the trace for the fermions.

2.1 Zero temperature: Euclidean AdS_{d+1}

In this section we compute the trace (2.5) for fermions at zero temperature. We begin by reviewing the solution to the following eigenvalue equation

$$\mathcal{D}\psi = i\lambda\psi. \quad (2.6)$$

We shall be using metric of AdS_{d+1} in Poincaré coordinates

$$ds^2 = \frac{L^2}{y^2} (dy^2 + \eta_{\mu\nu} dx^\mu dx^\nu). \quad (2.7)$$

In these coordinates, $\epsilon_a^M = y\delta_a^M$ and $\omega_M^{bc} = (\delta_y^a \delta_M^b - \delta_M^a \delta_y^b)/y$. Thus $\mathcal{D} = y\Gamma^a \partial_a - \frac{d}{2}\Gamma_y$. Writing the Dirac fermion ψ as

$$\psi = \begin{pmatrix} a_+ \psi_+ \\ a_- \psi_- \end{pmatrix} \quad (2.8)$$

where $\Gamma_y \psi_\pm = \pm \psi_\pm$. When $d+1$ is even ψ_\pm are of $2^{\frac{d-1}{2}}$ components and a_\pm are $2^{\frac{d-1}{2}} \times 2^{\frac{d-1}{2}}$ constant matrices, to be determined later. We have thus the following first order differential equations

$$\begin{aligned} a_+ y \partial_y \psi_+ - a_+ \frac{d}{2} \psi_+ + a_- y \Gamma_i \partial_i \psi_- &= i\lambda \psi_+ a_+ \\ -a_- y \partial_y \psi_- + a_- \frac{d}{2} \psi_- + a_+ y \Gamma_i \partial_i \psi_+ &= i\lambda \psi_- a_- \end{aligned} \quad (2.9)$$

The above equations lead to a decoupled set of second order differential equations which on rescaling $\psi_\pm = y^{\frac{d+1}{2}} \tilde{\psi}_\pm$ and further writing $\tilde{\psi}_\pm(\vec{x}, y) = e^{i\vec{k}\cdot\vec{x}} \tilde{\psi}_\pm(y)$ have the following form

$$y^2 \partial_y^2 \tilde{\psi}_\pm + y \partial_y \tilde{\psi}_\pm - \left[k^2 y^2 + (i\lambda \mp \frac{1}{2})^2 \right] \tilde{\psi}_\pm = 0. \quad (2.10)$$

The solutions to (2.10) are given by modified Bessel functions $\tilde{\psi}_{\pm}(ky) = (ky)^{\frac{d+1}{2}} K_{i\lambda \mp \frac{1}{2}}(ky)$. The solution must satisfy the Dirac equation (2.6), this gives

$$i\Gamma_i k_i a_+ = k a_- \quad (2.11)$$

leading to the following form of the eigenfunctions [28]

$$\psi_{\vec{k},\lambda}(\vec{x}, y) = \left(\begin{array}{c} \tilde{\psi}_+(ky) \\ \frac{i\Gamma_i k_i}{k} \tilde{\psi}_-(ky) \end{array} \right) e^{i\vec{k}\cdot\vec{x}}. \quad (2.12)$$

For each pair of ψ_{\pm} , the eigenfunctions are normalized as

$$\begin{aligned} & \int d^{d+1}x \sqrt{g} \psi_{\vec{k}',\lambda'}^{\dagger}(\vec{x}, y) \psi_{\vec{k},\lambda}(\vec{x}, y) \\ &= \int d^{d+1}x e^{i(\vec{k}-\vec{k}')\cdot\vec{x}} (k'k)^{\frac{d+1}{2}} \left[K_{i\lambda-\frac{1}{2}}(ky) K_{-i\lambda'-\frac{1}{2}}(k'y) + K_{i\lambda+\frac{1}{2}}(ky) K_{-i\lambda'+\frac{1}{2}}(k'y) \right] \\ &= (2\pi)^d \delta^d(\vec{k}-\vec{k}') k^d \delta(\lambda-\lambda') / \mu(\lambda) \end{aligned} \quad (2.13)$$

where

$$\mu(\lambda) = \frac{1}{\pi \Gamma(\frac{1}{2} + i\lambda) \Gamma(\frac{1}{2} - i\lambda)} = \frac{1}{\pi^2} \cosh(\pi\lambda) \quad (2.14)$$

as shown in appendix A.1. We can now compute the required trace (2.5) as follows.

$$\text{tr} \left[\frac{1}{\not{D} + M_f} \right] = \int d^{d+1}x \sqrt{g} \int \frac{d^d k}{(2\pi)^d} \frac{1}{k^d} \int_{-\infty}^{\infty} \frac{d\lambda}{i\lambda + M_f} \mu(\lambda) \psi_{\vec{k},\lambda}^{\dagger}(\vec{x}, y) \psi_{\vec{k},\lambda}(\vec{x}, y) \quad (2.15)$$

$$\begin{aligned} &= 2^{\frac{d-1}{2}} M_f \int d^{d+1}x \sqrt{g} \int \frac{d^d k}{(2\pi)^d} \frac{1}{k^d} \int_{-\infty}^{\infty} \frac{d\lambda}{\lambda^2 + M_f^2} \mu(\lambda) \times \\ &\times (ky)^{d+1} \left[K_{i\lambda-\frac{1}{2}}(ky) K_{-i\lambda-\frac{1}{2}}(ky) + K_{i\lambda+\frac{1}{2}}(ky) K_{-i\lambda+\frac{1}{2}}(ky) \right] \end{aligned} \quad (2.16)$$

$$= \frac{\mathcal{V}_{d+1} 2^{\frac{d+1}{2}} M_f}{(4\pi)^{(d+1)/2} \Gamma(\frac{d+1}{2})} \int_{-\infty}^{\infty} \frac{d\lambda}{\lambda^2 + M_f^2} \frac{\Gamma(\frac{d+1}{2} + i\lambda) \Gamma(\frac{d+1}{2} - i\lambda)}{\Gamma(\frac{1}{2} + i\lambda) \Gamma(\frac{1}{2} - i\lambda)} \quad (2.17)$$

$$= \text{sgn}(M_f) \frac{\mathcal{V}_{d+1} 2^{\frac{d+1}{2}}}{(4\pi)^{(d+1)/2}} \frac{\Gamma(\frac{d+1}{2} + |M_f|) \Gamma(\frac{1}{2} - \frac{d}{2})}{\Gamma(\frac{1}{2} - \frac{d}{2} + |M_f|)} \quad (2.18)$$

The factor of $2^{\frac{d-1}{2}}$ in the second line (2.16) comes from the number of components of $\psi_{\pm}(ky)$ for odd d . For even d this factor needs to be replaced by $2^{\frac{d-2}{2}}$. The third line (2.17) is obtained after performing the integral over k and putting in the measure $\mu(\lambda)$ from (2.14). Equation (2.17) contains the degeneracy for the eigenvalues $\pm i\lambda$ computed in [26]. Finally in the last line (2.18) we

have performed the integral over λ by closing the contour in the upper half complex λ plane (see A.2 for details) recovering the result in [14]. An alternate computation of the trace reversing the order of k and λ integrals is discussed in appendix A.3.

2.2 Finite temperature: Thermal AdS₃

In this section we consider thermal AdS _{$d+1$} which is the quotient space $\mathbb{H}^{d+1}/\mathbb{Z}$. Having got the eigenfunctions on Euclidean AdS _{$d+1$} we can now proceed with the analysis for thermal AdS _{$d+1$} following [15]. Define

$$\Psi_{\vec{k},\lambda}(x) = \frac{1}{\mathcal{N}} \sum_{n=-\infty}^{\infty} \mathcal{R}(\gamma^n) \psi_{\vec{k},\lambda}(\gamma^n x) \quad (2.19)$$

where $\gamma^n \in \mathbb{Z}$. \mathcal{N} is a normalization constant which regularizes the sum ¹. $\psi_{\vec{k},\lambda}(\gamma^n x)$ are eigenfunctions on \mathbb{H}^{d+1} (2.12). $\mathcal{R}(\gamma^n)$ is a one dimensional representation of the group \mathbb{Z} and can be written as $\mathcal{R}(\gamma^n) = e^{2\pi i n a}$ with $a = 1$ for bosons and $a = \frac{1}{2}$ for fermions. $\Psi_{\vec{k},\lambda}(x)$ by construction are eigenfunctions on the quotient space. The expression (2.19) is a generalization of the expression in [15]. For fermions we thus have $\Psi_{\vec{k},\lambda}(\gamma x) = -\Psi_{\vec{k},\lambda}(x)$.

Let us now first specialize to the case of thermal AdS₃ which is \mathbb{H}^3/\mathbb{Z} with the metric

$$ds^2 = \frac{L^2}{y^2} (dy^2 + dzd\bar{z}) \quad (2.20)$$

The action of γ^n on the coordinates as,

$$\gamma^n(y, z) = (e^{-n\beta}y, e^{2\pi i n\tau}z) \quad \text{where} \quad \tau = \frac{1}{2\pi}(\theta + i\beta) \quad (2.21)$$

In terms of real coordinates $z = x_1 + ix_2$, the action of the group element on the real coordinates $\vec{x} = (x_1, x_2)$ can be written as,

$$\gamma^n \vec{x} = \left(e^{-n\beta}(x_1 \cos n\theta - x_2 \sin n\theta), e^{-n\beta}(x_1 \sin n\theta + x_2 \cos n\theta) \right) \quad (2.22)$$

In three dimensions $\psi_{\vec{k},\lambda}(\vec{x}, y)$ is two dimensional. The normalization is worked out from $\psi_{\vec{k},\lambda}(\vec{x}, y)$ as follows,

$$\int d^3x \sqrt{g} \psi_{\vec{k},\lambda}^\dagger(\gamma^n x) \psi_{\vec{k}',\lambda'}(\gamma^{n'} x) \quad (2.23)$$

¹ \mathcal{N} is equal to $|\mathbb{Z}|$ which being infinite will be assumed to be regularized using some scheme.

$$\begin{aligned}
&= \int d^3x \sqrt{g} (ke^{-n\beta}y)^{3/2} (k'e^{-n'\beta}y)^{3/2} e^{-i\vec{k}\cdot(\gamma^n \vec{x})} e^{i\vec{k}'\cdot(\gamma^{n'} \vec{x})} \times \\
&\times \left[K_{-i\lambda-\frac{1}{2}}(ke^{-n\beta}y) K_{i\lambda'-\frac{1}{2}}(k'e^{-n'\beta}y) + K_{-i\lambda+\frac{1}{2}}(ke^{-n\beta}y) K_{i\lambda'+\frac{1}{2}}(k'e^{-n'\beta}y) \right] \quad (2.24)
\end{aligned}$$

$$\begin{aligned}
&= \int dy (ke^{-n\beta})^{3/2} (k'e^{-n'\beta})^{3/2} (2\pi)^2 \delta^2(\gamma^n \vec{k} - \gamma^{n'} \vec{k}') \times \\
&\times \left[K_{-i\lambda-\frac{1}{2}}(ke^{-n\beta}y) K_{i\lambda'-\frac{1}{2}}(k'e^{-n'\beta}y) + K_{-i\lambda+\frac{1}{2}}(ke^{-n\beta}y) K_{i\lambda'+\frac{1}{2}}(k'e^{-n'\beta}y) \right] \quad (2.25)
\end{aligned}$$

$$= (ke^{-(n-n')\beta})^2 (2\pi)^2 \delta^2(\gamma^{n-n'} \vec{k} - \vec{k}') \delta(\lambda - \lambda') / \mu(\lambda). \quad (2.26)$$

In the above equation (2.24), the integration over \vec{x} leads to the delta function which is then rewritten using the identity

$$\delta^2(\gamma^n \vec{k} - \gamma^{n'} \vec{k}') = e^{2n'\beta} \delta^2(\gamma^{(n-n')} \vec{k} - \vec{k}') \quad (2.27)$$

The action of γ^n on \vec{k} is defined as,

$$\gamma^n \vec{k} = \left(e^{-n\beta} (k_1 \cos n\theta + k_2 \sin n\theta), e^{-n\beta} (k_2 \cos n\theta - k_1 \sin n\theta) \right)$$

so that $|\gamma^n \vec{k}| = e^{-n\beta} k$. In equation (2.25) the y -integral is performed as shown in A.1.

The trace (2.5) for thermal AdS₃ can now be computed noting the fact that $\psi_{\vec{k},\lambda}(\gamma^n x)$ for $n \neq 0$ are also eigenfunctions of the Dirac operator with eigenvalues $\pm i\lambda$. The computation of trace for fermion is similar to that of scalars with some modifications, the details of which are as follows.

$$\text{tr} \left[\frac{1}{\not{D} + M_f} \right] = \frac{1}{\mathcal{N}^2} \sum_{n,n'} \int d^3x \sqrt{g} \int \frac{d^2k}{(2\pi)^2} \frac{1}{k^2} \int_{-\infty}^{\infty} \frac{d\lambda}{i\lambda + M_f} \mu(\lambda) \Psi_{\vec{k},\lambda}^\dagger(\vec{x}, y) \Psi_{\vec{k},\lambda}(\vec{x}, y) \quad (2.28)$$

$$= \frac{1}{\mathcal{N}^2} \sum_{n,n'} e^{-i\pi(n-n')} \int d^3x \sqrt{g} \int \frac{d^2k}{(2\pi)^2} \frac{1}{k^2} \int_{-\infty}^{\infty} \frac{d\lambda}{\lambda^2 + M_f^2} \mu(\lambda) M_f (ke^{-n\beta}y)^{3/2} (k'e^{-n'\beta}y)^{3/2} \times \quad (2.29)$$

$$\times \left[K_{-i\lambda-\frac{1}{2}}(ke^{-n\beta}y) K_{i\lambda-\frac{1}{2}}(k'e^{-n'\beta}y) + K_{-i\lambda+\frac{1}{2}}(ke^{-n\beta}y) K_{i\lambda+\frac{1}{2}}(k'e^{-n'\beta}y) \right] e^{i\vec{k}\cdot(\gamma^n \vec{x})} e^{-i\vec{k}'\cdot(\gamma^{n'} \vec{x})}$$

$$= \frac{2}{\mathcal{N}} \sum_n (-1)^n \frac{e^{-3n\beta/2}}{|1 - e^{2\pi i n \tau}|^2} \int_0^\infty \frac{dy}{y} \int_{-\infty}^{\infty} \frac{d\lambda}{\lambda^2 + M_f^2} \mu(\lambda) M_f \times$$

$$\times \int \frac{d^2k}{(2\pi)^2} (ky) \left[K_{-i\lambda-\frac{1}{2}}(ke^{-n\beta}y) K_{i\lambda-\frac{1}{2}}(ky) + K_{-i\lambda+\frac{1}{2}}(ke^{-n\beta}y) K_{i\lambda+\frac{1}{2}}(ky) \right] (2\pi)^2 \delta^2(\vec{k}) \quad (2.30)$$

We have made several simplifications in going from (2.29) and (2.30). The integral over \vec{x} which results in a delta function has been rewritten using

$$\delta^2(\gamma^n \vec{k} - \gamma^{n'} \vec{k}') = \frac{e^{2n'\beta}}{|1 - e^{2\pi i(n-n')\tau}|^2} \delta^2(\vec{k}) \quad (2.31)$$

y has been re-scaled $y \rightarrow e^{n'\beta}y$ within each term in the summation. The summation over n' cancels a factor of \mathcal{N} as each term in the summation over n' gives the same series in n . The factor of 2 in front in (2.30) is as a result of the symmetry of the trace under $n \rightarrow -n$. We have also excluded the zero temperature $n = 0$ term which has already been computed in (2.18).

The k integral in (2.30) gives the following

$$(ky) \left[K_{-i\lambda-\frac{1}{2}}(ke^{-n\beta}y)K_{i\lambda-\frac{1}{2}}(ky) + K_{-i\lambda+\frac{1}{2}}(ke^{-n\beta}y)K_{i\lambda+\frac{1}{2}}(ky) \right] \\ \xrightarrow{k \rightarrow 0} \frac{1}{2} \underbrace{\Gamma(1/2 - i\lambda) \Gamma(1/2 + i\lambda)}_{(\pi\mu(\lambda))^{-1}} \left[\left(e^{-n\beta} \right)^{-1/2-i\lambda} + \left(e^{-n\beta} \right)^{-1/2+i\lambda} \right] \quad (2.32)$$

We can now perform the λ integral by closing the contour in the upper/lower half complex λ plane. Both the terms in (2.32) are related to each other by $\lambda \rightarrow -\lambda$. The measure $\mu(\lambda)$ being an even function, they give the same contribution.

Thus

$$\text{tr} \left[\frac{1}{\mathcal{D} + M_f} \right] = \frac{2}{\mathcal{N}} \sum_n (-1)^n \text{sgn}(M_f) \frac{e^{-n\beta(1+|M_f|)}}{|1 - e^{2\pi i n \tau}|^2} \int_0^\infty \frac{dy}{y} \quad (2.33)$$

The divergence in the integral over y is taken care of as follows: noting that the fundamental region along y is $e^{-\beta} \leq y \leq 1$,

$$\int_0^\infty \frac{dy}{y} = \sum_{m=-\infty}^\infty \int_{e^{-(m+1)\beta}}^{e^{-m\beta}} \frac{dy}{y} = \mathcal{N}\beta. \quad (2.34)$$

The finite temperature contribution to the one-loop partition function is then

$$\log Z_\tau^{(1)} = - \int_{M_f}^\infty \text{tr} \left[\frac{1}{\mathcal{D} + M} \right] dM \quad (2.35)$$

$$= -2 \sum_{n=1}^\infty \frac{(-1)^n}{n} \frac{e^{-n\beta(1+|M_f|)}}{|1 - e^{2\pi i n \tau}|^2} \quad (2.36)$$

Denoting $q = e^{2\pi i \tau}$, and $\Delta = |M_f| + 1$ we can rewrite (2.36) as

$$\log Z_\tau^{(1)} = -2 \sum_{n=1}^\infty \sum_{l,l'=0}^\infty \frac{(-1)^n}{n} q^{n(l+\Delta/2)} \bar{q}^{n(l'+\Delta/2)} \quad (2.37)$$

$$= 2 \sum_{l,l'=0}^\infty \log \left(1 + q^{(l+\Delta/2)} \bar{q}^{(l'+\Delta/2)} \right) \quad (2.38)$$

$$= 2 \sum_{l=0}^{\infty} (l+1) \log \left(1 + e^{-\beta(\Delta+l)} \right) \quad \text{for } \theta = 0. \quad (2.39)$$

Δ is the dimension of the operator in the boundary dual to the fermion in AdS_3 . From the boundary CFT point of view the contribution to the partition function comes from the primary operator of dimension Δ and well as its descendants of dimensions $\Delta + l$.

2.2.1 Thermal AdS_{d+1}

We now generalize the computation for AdS_3 to that of higher dimensional spaces. We first consider the case for even d . The metric is written as

$$ds^2 = \frac{L^2}{y^2} \left(dy^2 + \sum_{i=1}^{d/2} dz_i d\bar{z}_i \right). \quad (2.40)$$

For thermal AdS_{d+1} the action of γ_i^n on the coordinates is,

$$\gamma_i^n(y, z_i) = (e^{-n\beta} y, e^{2\pi i n \tau_i} z_i) \quad \text{where} \quad \tau_i = \frac{1}{2\pi} (\theta_i + i\beta). \quad (2.41)$$

Next define real coordinates $z_i = x_{i1} + ix_{i2}$. The action on the real coordinates $\vec{x}_i = (x_{i1}, x_{i2})$ can be written as in equation (2.22) with θ replaced by θ_i . In odd $(d+1)$ dimensions $\psi_{\vec{k}, \lambda}(\vec{x}, y)$ is $2^{(d-2)/2}$ dimensional. For each pair of the eigenfunctions, the normalization is worked out from $\psi_{\vec{k}, \lambda}(\vec{x}, y)$ as follows,

$$\int d^{d+1} x \sqrt{g} \psi_{\vec{k}, \lambda}^\dagger(\gamma^n x) \psi_{\vec{k}', \lambda'}(\gamma^{n'} x) \quad (2.42)$$

$$= \int d^{d+1} x \sqrt{g} (ke^{-n\beta} y)^{(d+1)/2} (k'e^{-n'\beta} y)^{(d+1)/2} e^{-i\vec{k}_i \cdot (\gamma_i^n \vec{x}_i)} e^{i\vec{k}'_i \cdot (\gamma_i^{n'} \vec{x}_i)} \\ \times \left[K_{-i\lambda - \frac{1}{2}}(ke^{-n\beta} y) K_{i\lambda' - \frac{1}{2}}(k'e^{-n'\beta} y) + K_{-i\lambda + \frac{1}{2}}(ke^{-n\beta} y) K_{i\lambda' + \frac{1}{2}}(k'e^{-n'\beta} y) \right] \quad (2.43)$$

$$= \int dy (ke^{-n\beta})^{1/2} (k'e^{-n'\beta})^{1/2} \left[K_{-i\lambda - \frac{1}{2}}(ke^{-n\beta} y) K_{i\lambda' - \frac{1}{2}}(k'e^{-n'\beta} y) + K_{-i\lambda + \frac{1}{2}}(ke^{-n\beta} y) K_{i\lambda' + \frac{1}{2}}(k'e^{-n'\beta} y) \right] \\ \times \prod_{i=1}^{d/2} (ke^{-n\beta})(k'e^{-n'\beta})(2\pi)^2 \delta^2(\gamma_i^n \vec{k} - \gamma_i^{n'} \vec{k}') \quad (2.44)$$

$$= \delta(\lambda - \lambda') / \mu(\lambda) \prod_{i=1}^{d/2} (ke^{-(n-n')\beta})^2 (2\pi)^2 \delta^2(\gamma_i^{n-n'} \vec{k} - \vec{k}'). \quad (2.45)$$

In the above equation (2.43), the integration over \vec{x} leads to the delta function which is then rewritten using the identity (2.27). In equation (2.44) the y -integral is performed as shown in A.1.

The trace can now be computed following the steps as in AdS₃.

$$\text{tr} \left[\frac{1}{\not{D} + M_f} \right] = \frac{1}{\mathcal{N}^2} \sum_{n,n'} \int d^{d+1}x \sqrt{g} \int \frac{d^d k}{(2\pi)^d} \frac{1}{k^d} \int_{-\infty}^{\infty} \frac{d\lambda}{i\lambda + M_f} \mu(\lambda) \Psi_{\vec{k},\lambda}^\dagger(\vec{x}, y) \Psi_{\vec{k},\lambda}(\vec{x}, y) \quad (2.46)$$

$$\begin{aligned} &= \frac{2^{\frac{(d-2)}{2}}}{\mathcal{N}^2} \sum_{n,n'} e^{-i\pi(n-n')} \int d^{d+1}x \sqrt{g} \int \frac{d^d k}{(2\pi)^d} \frac{1}{k^d} \int_{-\infty}^{\infty} \frac{d\lambda}{\lambda^2 + M_f^2} \mu(\lambda) M_f (ke^{-n\beta}y)^{(d+1)/2} (ke^{-n'\beta}y)^{(d+1)/2} \\ &\times \left[K_{-i\lambda-\frac{1}{2}}(ke^{-n\beta}y) K_{i\lambda-\frac{1}{2}}(ke^{-n'\beta}y) + K_{-i\lambda+\frac{1}{2}}(ke^{-n\beta}y) K_{i\lambda+\frac{1}{2}}(ke^{-n'\beta}y) \right] e^{i\vec{k}_i \cdot (\gamma_i^{n'} \vec{x}_i)} e^{-i\vec{k}_i \cdot (\gamma_i^n \vec{x}_i)} \end{aligned} \quad (2.47)$$

$$\begin{aligned} &= \frac{1}{\mathcal{N}} \sum_n (-1)^n \int_0^\infty \frac{dy}{y} \int \frac{d^d k}{(2\pi)^d} (ky) e^{-n\beta/2} \int_{-\infty}^{\infty} \frac{d\lambda}{\lambda^2 + M_f^2} \mu(\lambda) M_f \\ &\times \left[K_{-i\lambda-\frac{1}{2}}(ke^{-n\beta}y) K_{i\lambda-\frac{1}{2}}(ky) + K_{-i\lambda+\frac{1}{2}}(ke^{-n\beta}y) K_{i\lambda+\frac{1}{2}}(ky) \right] \\ &\times \prod_{i=1}^{d/2} \frac{2e^{-n\beta}}{|1 - e^{2\pi i n \tau_i}|^2} (2\pi)^2 \delta^2(\vec{k}_i) \end{aligned} \quad (2.48)$$

We have again made simplifications in going from (2.47) and (2.48) similar to that of AdS₃ and have used the identities (2.27) and (2.31). The k , λ and y integrals can be computed as before. This results in the following expression for the finite temperature contribution to the one-loop partition function

$$\log Z_\tau^{(1)} = - \int_{M_f}^\infty \text{tr} \left[\frac{1}{\not{D} + M} \right] dM \quad (2.49)$$

$$= - \sum_{n=1}^\infty \frac{(-1)^n}{n} e^{-n\beta|M_f|} \prod_{i=1}^{d/2} \frac{2e^{-n\beta}}{|1 - e^{2\pi i n \tau_i}|^2} \quad (2.50)$$

Denoting $q = e^{2\pi i \tau}$, and $\Delta = |M_f| + d/2$ we can rewrite (2.50) as

$$\log Z_\tau^{(1)} = - \sum_{n=1}^\infty \prod_{i=1}^{d/2} \sum_{l_i, l'_i=0}^\infty 2 \frac{(-1)^n}{n} q_i^{n(l_i+\Delta/d)} \bar{q}_i^{n(l'_i+\Delta/d)} \quad (2.51)$$

$$= 2^{d/2} \sum_{\substack{l_1, l'_1 \\ l_{d/2}, l'_{d/2}=0}}^\infty \log \left(1 + q_1^{(l_1+\Delta/d)} \bar{q}_1^{(l'_1+\Delta/d)} \dots q_{d/2}^{(l_{d/2}+\Delta/d)} \bar{q}_{d/2}^{(l'_{d/2}+\Delta/d)} \right) \quad (2.52)$$

$$= 2^{d/2} \sum_{\substack{l_1, l'_1 \\ l_{d/2}, l'_{d/2}=0}}^\infty \log \left(1 + e^{-\beta(l_1+l'_1+\dots+l_{d/2}+l'_{d/2}+\Delta)} \right) \quad \text{for } \theta_i = 0 \quad (2.53)$$

$$= 2^{d/2} \sum_{l=0}^{\infty} g(l, d) \log \left(1 + e^{-\beta(\Delta+l)} \right) \quad \text{where} \quad g(l, d) = \frac{(d+l-1)!}{l!(d-1)!} \quad (2.54)$$

The metric for odd d is written as

$$ds^2 = \frac{L^2}{y^2} \left(dy^2 + \sum_{i=1}^{(d-1)/2} dz_i d\bar{z}_i + dx_d^2 \right). \quad (2.55)$$

The action of γ^n on the coordinates is,

$$\gamma^n(y, z_i, x_d) = (e^{-n\beta} y, e^{2\pi i n \tau_i} z_i, e^{-n\beta} x_d) \quad \text{where} \quad \tau_i = \frac{1}{2\pi}(\theta_i + i\beta). \quad (2.56)$$

For odd d the fermion wave function has $2^{(d-1)/2}$ components. The normalization for a pair of fermions is as follows,

$$\begin{aligned} & \int d^{d+1}x \sqrt{g} \psi_{\vec{k}, \lambda}^\dagger(\gamma^n x) \psi_{\vec{k}', \lambda'}(\gamma^{n'} x) \\ &= (k e^{-(n-n')\beta}) (2\pi) \delta(\gamma^{n-n'} \vec{k} - \vec{k}') \prod_{i=1}^{(d-1)/2} (k e^{-(n-n')\beta})^2 (2\pi)^2 \delta^2(\gamma^{n-n'} \vec{k} - \vec{k}') \delta(\lambda - \lambda') / \mu(\lambda). \end{aligned} \quad (2.57)$$

The finite temperature contribution to the one-loop partition function following computations similar to the previous cases is

$$\log Z_\tau^{(1)} = - \sum_{n=1}^{\infty} \frac{(-1)^n}{n} \frac{2e^{-n\beta(|M_f|+1/2)}}{|1 - e^{-n\beta}|} \prod_{i=1}^{(d-1)/2} \frac{2e^{-n\beta}}{|1 - e^{2\pi i n \tau_i}|^2} \quad (2.58)$$

$$= 2^{(d+1)/2} \sum_{\substack{l_1, l'_1 \\ \vdots \\ l_d=0}}^{\infty} \log \left(1 + q_1^{(l_1+\Delta'/(d-1))} \bar{q}_1^{(l'_1+\Delta'/(d-1))} \dots q_{(d-1)/2}^{(l_{(d-1)/2}+\Delta'/(d-1))} \bar{q}_{(d-1)/2}^{(l'_{(d-1)/2}+\Delta'/(d-1))} |q_d|^{(1/2+l_d)} \right)$$

$$= 2^{(d+1)/2} \sum_{\substack{l_1, l'_1 \\ \vdots \\ l_d=0}}^{\infty} \log \left(1 + e^{-\beta(l_1+l'_1+\dots+l_{(d-1)/2}+l'_{(d-1)/2}+l_d+\Delta)} \right) \quad \text{for } \theta_i = 0 \quad (2.59)$$

$$= 2^{(d+1)/2} \sum_{l=0}^{\infty} g(l, d) \log \left(1 + e^{-\beta(\Delta+l)} \right). \quad (2.60)$$

where $\Delta' = \Delta - 1/2$ and Δ is given above equation (2.51). $g(l, d)$ is given in equation (2.54)

3 Study of theories with fermions

In this section we study the phases of Yukawa theory for $d = 1, 2, 3$ and the massive Gross-Neveu models for $d = 1, 2$. In AdS₄ we also discuss the Gross-Neveu-Yukawa model. The phases are studied by writing down the effective potential utilizing the results from the previous sections for the fermion trace and those of scalars from [15]. As already seen in the study of phases with only scalars, unlike the finite temperature piece, the zero temperature contribution to the trace is proportional to the divergent volume of Euclidean AdS space. This divergence needs to be regulated. In the cutoff scheme these renormalized volumes are $\mathcal{V}_2 = -\beta$, $\mathcal{V}_3 = -\pi\beta/2$, $\mathcal{V}_4 = 2\pi\beta/3$ (see [15] and references therein). The renormalized volume for AdS₃ differs both in magnitude and in sign from the above in the the dimensional regularization scheme [33]. The results for the phases corresponding to the positive regularized volume of AdS₃ will thus differ from those presented here. Though this modification can be easily implemented as in [15], we have however not used this in our analysis below.

For the numerical computations in the following sections, we have set $n_{\max} = 10$ for the sum in the finite temperature contributions (2.35),(2.49),(2.58). In fact the series converges within the first two terms up to at least four decimal places because of the exponential damping.

3.1 Yukawa theory

The general form of the effective potential is given by

$$\begin{aligned}
 V_{eff} = & \frac{1}{2}m_s^2\phi_{cl}^2 + \frac{\lambda_3}{3!}\phi_{cl}^3 + \frac{\lambda_4}{4!}\phi_{cl}^4 + \lambda_1\phi_{cl} - \frac{1}{2\mathcal{V}_{d+1}} \int_{M_s^2}^{\infty} \text{tr} \left[\frac{1}{-\square_E + M_s^2} \right] dM_s^2 \\
 & - \frac{1}{\mathcal{V}_{d+1}} \int_0^{M_f} \text{tr} \left[\frac{1}{\not{D} + M_f} \right] dM_f + \text{counterterms}
 \end{aligned} \tag{3.61}$$

$$\text{where } M_s^2 = m_s^2 + \lambda_3\phi_{cl} + \frac{\lambda_4}{2}\phi_{cl}^2 \quad \text{and} \quad M_f = m_f + g\phi_{cl}. \tag{3.62}$$

In the absence of the $\phi \rightarrow -\phi$ symmetry, the linear and cubic terms in ϕ need to be included. The zero temperature contribution to the traces (2.18) have poles corresponding to UV divergence for odd d , which in our case is $d = 1, 3$. For these values of d , the counterterms cancel the UV divergences coming from the trace. $m_s, \lambda_3, \lambda_4, \lambda_1, g$ and m_f appearing in (3.61) are thus renormalized parameters. To be more specific, at one loop level, only bare values of $m_s, \lambda_3, \lambda_4$ and λ_1 , get renormalized by the counterterms in (3.61). Bare values of m_f and g would be assumed to be renormalized at one-loop level by counterterms corresponding to fermion propagator and the Yukawa vertex.

In the following sections we use a scheme in which counterterms are evaluated using suitable renormalization conditions. This we do only for the divergent n -point scalar terms. For example one and two-point for $d = 1$ and one to four-point for $d = 3$. Correspondingly the scheme renormalizes m_s and λ_1 for $d = 1$ and $m_s, \lambda_3, \lambda_4$ and λ_1 for $d = 3$. The linear term in ϕ_{cl} can be removed by setting a renormalization condition so that the tadpole vanishes. Thus the renormalized one-point coupling λ_1 will be set to zero. An alternate renormalization scheme that is similar to the Minimal Subtraction scheme is discussed for $d = 1, 3$ in appendix B.2.

3.1.1 AdS₃

The zero temperature contribution from the trace (2.18) has no pole for $d = 2$ and is given by

$$\frac{1}{\mathcal{V}_3} \text{tr} \frac{1}{\not{D} + M_f} = -\frac{1}{2\pi} \text{sgn}(M_f) \left(M_f^2 - \frac{1}{4} \right) \quad (3.63)$$

Including the contribution from the scalar determinant, the effective potential at zero temperature is

$$V_{eff}^0 = \frac{1}{2} m_s^2 \phi_{cl}^2 + \frac{\lambda_3}{3!} \phi_{cl}^3 + \frac{\lambda_4}{4!} \phi_{cl}^4 + \lambda_1 \phi_{cl} - \frac{\nu^3}{12\pi} + \frac{1}{2\pi} \left(\frac{|M_f|^3}{3} - \frac{|M_f|}{4} \right) \quad (3.64)$$

where, $\nu = \sqrt{(d/2)^2 + M_s^2}$.

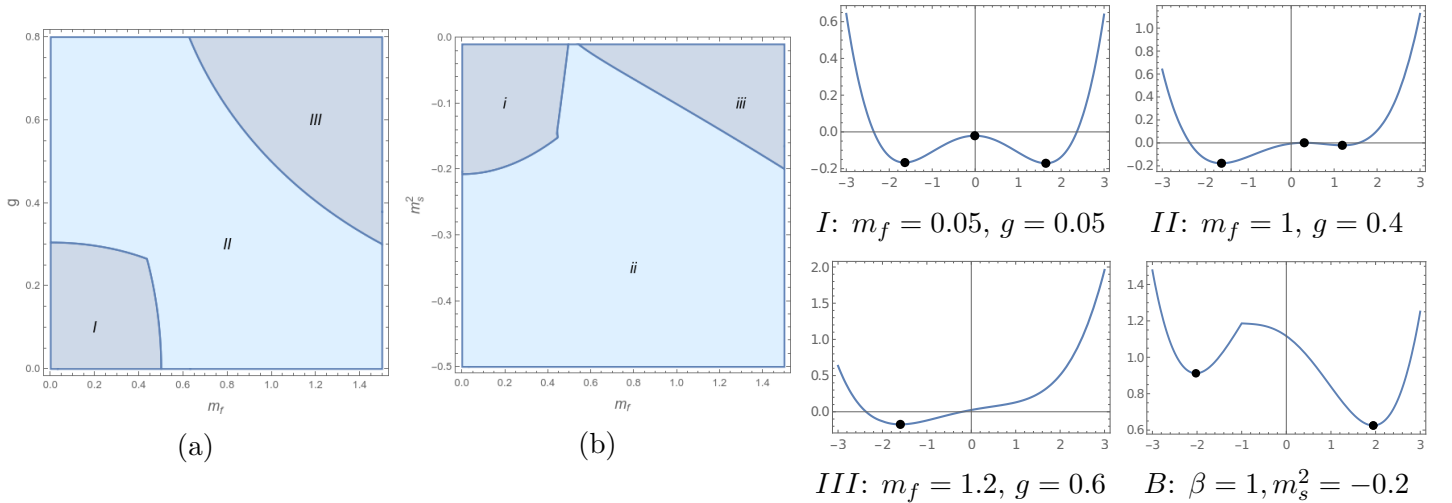


Figure 2: Regions in the m_f - g plane for $m_s^2 = -0.2$ (a), and m_f - m_s^2 plane for $g = 0.3$ (b). Various representative potentials (extreme right) at zero temperature. Black dots on the potential plots are the extrema. B is potential plot at finite temperature for region B in the finite temperature phase plot Figure 3a.

Figure 2 shows the regions in m_f - g , m_f - m_s^2 spaces and potential plots for a fixed value of $m_s^2 = -0.2$ at zero temperature. In the numerical plots we have set $\lambda_1 = \lambda_3 = 0$ and $\lambda_4 = 0.5$. Some essential features of the phases are discussed below.

1. For a fixed value of m_s^2 , there are in general three regions. Figure 2a shows the (m_f, g) space plot for $m_s^2 = -0.2$. In regions *I* and *II* there are two minima. Region *III* has only one minimum. The more negative m_s^2 is, the *II* region expands and the top right region diminishes in size where there is only one minimum. Figure 2b shows similar regions in the m_f - m_s^2 plane for a fixed value of $g = 0.3$.
2. There is a first-order transition line, the boundary separating regions *I* and *II* where the both the minima have same height. The sharp edge of the boundary is due to the presence of absolute values (cusp) in the potential (3.64) which lies between the left minimum and the maximum. At higher values of g and m_f , the right minimum ceases to exist in region *III*.
3. For a fixed value of m_f and g there is also a transition at some critical value of m_s^2 (similar to that of symmetric potential) when the two minima start appearing. Whether the left or the right is lower depends on the values of g and m_f .

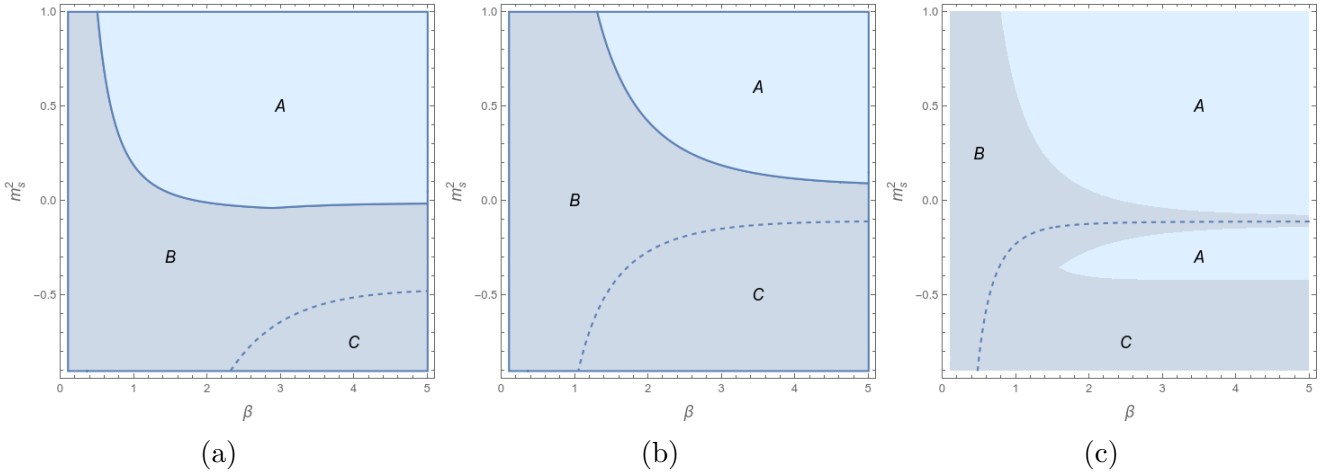


Figure 3: Phase plots in the $m_s^2 - \beta$ plane for (a) $m_f = 0.2$, $g = 0.2$ (b) $m_f = 0.1$, $g = 0.4$ (c) $m_f = 1$, $g = 0.8$ which are points in region *I*, *II* and *III* of the zero temperature plot (Figure 2a) respectively.

Inserting the finite temperature pieces,

$$V_{eff} = V_{eff}^0 + \frac{2}{\pi\beta} \sum_{n=1}^{\infty} \frac{1}{n} \frac{e^{-n\beta(1+\sqrt{1+M_s^2})}}{|1 - e^{-n\beta}|^2} - \frac{4}{\pi\beta} \sum_{n=1}^{\infty} \frac{(-1)^n}{n} \frac{e^{-n\beta(1+|M_f|)}}{|1 - e^{-n\beta}|^2} \quad (3.65)$$

The phase plots in the $m_s^2 - \beta$ plane for various values of (m_f, g) are shown in Figure 3. In all

the plots, region A has one minimum. Regions B and C have two minima which exchange dominance across the dashed lines. At the boundary of A a new minimum appears from either of the two branches of the potential satisfying $m_f + g\phi_{cl} > 0$ or $m_f + g\phi_{cl} < 0$. The regions B and C which have two minima are the union of all the regions coming from either of the branches. The asymptotic zero temperature m_s^2 values for the phase boundaries are given in Table 1.

Figure	m_{sA}^{2*}	m_{sB}^{2*}
3a	-0.014	-0.465
3b	0.079	-0.106
3c	-0.082, -0.133, -0.421	-0.109

Table 1: Zero temperature values of m_s^2 for phase boundaries. m_{sA}^{2*} is the zero temperature value for the boundary separating A and B in Figures 3a, 3b and boundary separating A - B and A - C in Figure 3c. m_{sB}^{2*} that of the dashed boundary separating B and C in all phase plots of Figure 3.

At finite temperature, starting from a (m_f, g) point with $m_s^2 = -0.2$ in the regions I , II and III of the zero-temperature phase plot (for example Figure 2a) we have the following.

1. At high temperatures the right minimum is always the global minimum. A point in region I (in Figure 2a) thus always has lower right minimum for all temperatures. This point lies in region B in Figure 3a. Points lying in region C undergoes transition across the dashed line as β is decreased.
2. A point in region II (in Figure 2a) lies in region C in Figure 3b. The potential undergoes change of dominance of the minima across the dashed line shown in Figure 3b.
3. If one starts from a point in region III (in Figure 2a), this point lies in region A of Figure 3c. At finite temperature the right minimum appears which is followed by a first-order phase transition beyond which it becomes the lowest minimum as temperature is increased further.

3.1.2 AdS₂

The zero temperature traces are UV divergent and can be regularized using dimensional regularization. Expanding about $d = 1$ with $\epsilon = 1 - d$, the zero temperature traces for the scalar from [15] and the fermions (from equation (2.18)) are

$$\frac{\mu^{-\epsilon}}{2\mathcal{V}_{d+1}} \text{tr} \frac{1}{-\square_E + M_s^2} = \frac{1}{4\pi\epsilon} + \frac{1}{8\pi} \left[-2\psi^{(0)} \left(\nu + \frac{1}{2} \right) - \gamma + \log(4\pi/\mu^2) \right] + \mathcal{O}(d-1) \quad (3.66)$$

$$\frac{\mu^{-\epsilon}}{\mathcal{V}_{d+1}} \text{tr} \frac{1}{\not{D} + M_f} = 4M_f \left[\frac{1}{4\pi\epsilon} - \frac{1}{8\pi} \left(\psi^{(0)}(|M_f|) + \psi^{(0)}(|M_f| + 1) + \gamma - \log(2\pi/\mu^2) \right) \right] + \mathcal{O}(d-1) \quad (3.67)$$

In terms of Feynman diagrams, the UV divergences arise from the two-point and the one-point diagrams. We thus use the following structure of the counterterms

$$\phi_{cl} \delta\lambda_1 + \frac{1}{2}\phi_{cl}^2 \delta m_s^2$$

with renormalization conditions

$$\left. \frac{\partial V_{eff}^0}{\partial \phi_{cl}} \right|_{\phi_{cl}=0} = 0 \quad \left. \frac{\partial^2 V_{eff}^0}{\partial \phi_{cl}^2} \right|_{\phi_{cl}=0} = m_s^2. \quad (3.68)$$

These give the following zero temperature effective potential

$$\begin{aligned} V_{eff}^0 &= \frac{1}{2}m_s^2\phi_{cl}^2 + \frac{\lambda_3}{3!}\phi_{cl}^3 + \frac{\lambda_4}{4!}\phi_{cl}^4 \\ &- \frac{1}{4\pi} \left[\int_{m_s^2}^{M_s^2} \psi^{(0)}(\nu(\phi_{cl}) + 1/2) dM_s^2 - \int_{m_f}^{M_f} 2M_f \left(\psi^{(0)}(|M_f|) + \psi^{(0)}(1 + |M_f|) \right) dM_f \right] \\ &+ \frac{1}{8\pi}\phi_{cl}^2 \left[\lambda_4\psi^{(0)}\left(\sqrt{1/4 + m_s^2} + 1/2\right) - 2g^2 \left(\psi^{(0)}(m_f) + \psi^{(0)}(1 + m_f) \right) \right. \\ &- \left. 2g^2 m_f \left(\psi^{(1)}(m_f) + \psi^{(1)}(1 + m_f) \right) + \frac{1}{2}\lambda_3^2 \frac{\psi^{(1)}\left(\sqrt{1/4 + m_s^2} + 1/2\right)}{\sqrt{1/4 + m_s^2}} \right] \\ &+ \frac{1}{8\pi}\phi_{cl} \left[2\lambda_3\psi^{(0)}\left(\sqrt{1/4 + m_s^2} + 1/2\right) - 4gm_f \left(\psi^{(0)}(m_f) + \psi^{(0)}(1 + m_f) \right) \right] \end{aligned} \quad (3.69)$$

We have set the lower limits of the integrals in the above expression as m_s^2 and m_f for the scalar and the fermion traces respectively. This sets V_{eff}^0 at $\phi_{cl} = 0$ equal to zero.

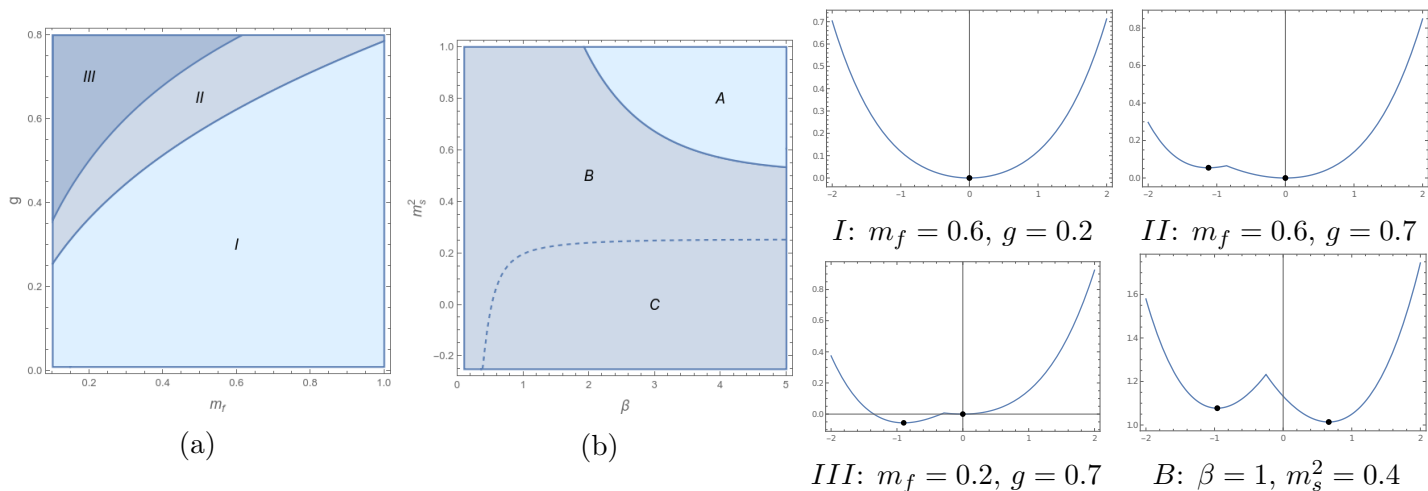


Figure 4: (a): Phases at zero temperature for $m_s^2 = 0.2$ in the m_f - g plane and representative potentials *I*, *II* and *III* (extreme right). (b): Regions in the β - m_s^2 plane for $m_f = 0.1$, $g = 0.4$ a point in region *III* in (a). A plot of the potential at finite temperature corresponding to region *B* in (b) is shown in the right. Black dots on the potential plots are the extrema.

The finite temperature effective potential using (2.58) and including the expression for scalars is

$$V_{eff} = V_{eff}^0 + \frac{1}{\beta} \sum_{n=1}^{\infty} \frac{1}{n} \frac{e^{-n\beta(1/2+\sqrt{1/4+M_s^2})}}{|1-e^{-n\beta}|} - \frac{2}{\beta} \sum_{n=1}^{\infty} \frac{(-1)^n e^{-n\beta(1/2+|M_f|)}}{|1-e^{-n\beta}|}. \quad (3.70)$$

The phases of this theory are summarized as follows. In the plots we have set $\lambda_3 = 0$ and $\lambda_4 = 0.5$.

1. The renormalization conditions (3.68) imply that at zero temperature the extremum at $\phi_{cl} = 0$ is either a maximum or a minimum which is determined by the sign of the scalar mass-squared, m_s^2 . When $m_s^2 < 0$, there are two minima. The left minimum is lower than the right for all values of m_f and g . When $m_s^2 > 0$, there is either a single minimum or two minima depending on the values of m_f and g and m_s^2 , see Figure 4a. Region *I* has one minimum. Two minima exchange dominance across the boundary separating regions *II* and *III*.

2. At finite temperatures, $\beta - m_s^2$ plots are shown in Figures 4b and 5a corresponding to a point in region *I* and *III* of Figure 4a respectively. In these phase plots, the region *A* has only one minimum. Regions *B* and *C* have two minima. Note that at zero temperature (large β), a (m_f, g) point (for $m_s^2 = 0.2$) corresponding to *I* and *III* lies in *A* and in *C* respectively.

3. The dashed lines separating regions *B* and *C* in Figures 4b and 5a are phase boundaries where the two minima exchange dominance. Potentials corresponding to representative points in these regions are shown in the extreme right plots of Figures 4 and 5. The relevant boundaries for $m_f = 0.1$ and various values of g are shown in Figure 5b. The asymptotic values of m_s^2 at zero temperature, m_{sA}^{2*} , m_{sB}^{2*} for the solid and dashed boundary curves respectively are given within the Figure 5b. The corresponding values in Figure 4b are $m_{sA}^{2*} = 0.4$, $m_{sB}^{2*} = 0.2$.

3.1.3 AdS₄

Expanding the zero temperature traces about $d = 3$ with $\epsilon = 3 - d$, from [15] we have

$$\frac{\mu^{-\epsilon}}{\mathcal{V}_{d+1}} \text{tr} \frac{1}{-\square + M_s^2} = \frac{(2 + M_s^2)}{16\pi^2} \left[-\frac{2}{\epsilon} - 1 + \gamma - \log(4\pi) + \psi^{(0)}\left(\nu - \frac{1}{2}\right) + \psi^{(0)}\left(\nu + \frac{3}{2}\right) + \log(\mu^2) \right] \quad (3.71)$$

and from (2.18)

$$\frac{\mu^{-\epsilon}}{\mathcal{V}_{d+1}} \text{tr} \frac{1}{\not{D} + M_f} = \frac{M_f(M_f^2 - 1)}{4\pi^2} \left[-\frac{2}{\epsilon} - 1 + \gamma - \log(2\pi) + \psi^{(0)}(|M_f| - 1) + \psi^{(0)}(|M_f| + 2) + \log(\mu^2) \right] \quad (3.72)$$

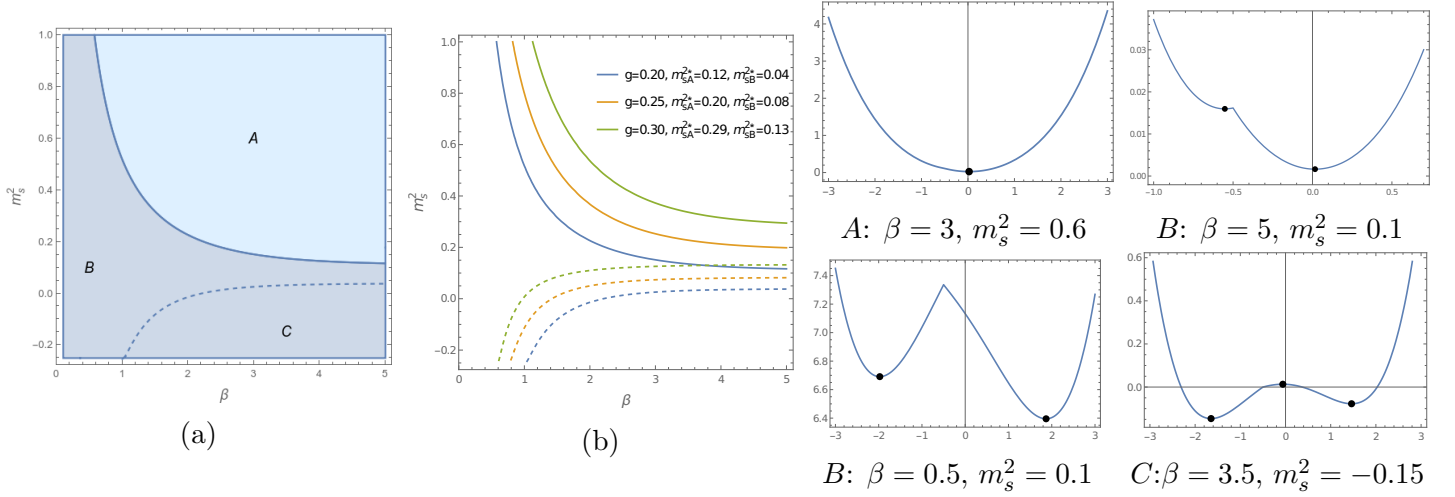


Figure 5: (a): Regions in the β - m_s^2 plane for $m_f = 0.1$, $g = 0.2$ and representative potentials (right). Black dots on the potential plots are the extrema. (b): Shows the phase boundaries for $m_f = 0.1$ and various values of g .

In four dimensions one to four point functions in ϕ_{cl} are UV divergent. Here again we use the renormalization scheme as in the previous section for AdS_2 . The counterterms have the following form

$$\phi_{cl} \delta\lambda_1 + \frac{1}{2}\phi_{cl}^2 \delta m_s^2 + \frac{1}{3!}\phi_{cl}^3 \delta\lambda_3 + \frac{1}{4!}\phi_{cl}^4 \delta\lambda_4$$

We use the with renormalization conditions at $\phi_{cl} = 0$

$$\frac{\partial V_{eff}^0}{\partial \phi_{cl}} = 0 \quad \frac{\partial^2 V_{eff}^0}{\partial \phi_{cl}^2} = m_s^2 \quad \frac{\partial^3 V_{eff}^0}{\partial \phi_{cl}^3} = \lambda_3 \quad \frac{\partial^4 V_{eff}^0}{\partial \phi_{cl}^4} = \lambda_4. \quad (3.73)$$

The expression for the effective potential V_{eff}^0 utilizing the above renormalization condition is quite long and can be found in equation (B.117) of appendix B.1. In the large ϕ_{cl} limit, the leading contributions from the scalar and the fermion to the potential come from the integrals in (B.117),

$$\frac{1}{2} \int_{m_s^2}^{M_s^2} \left(\frac{2 + M_s^2}{16\pi^2} \right) \left(\psi^{(0)} \left(\nu(\phi_{cl}) - \frac{1}{2} \right) + \psi^{(0)} \left(\nu(\phi_{cl}) + \frac{3}{2} \right) \right) dM_s^2 \sim \frac{\lambda_4^2}{128\pi^2} \phi_{cl}^4 \log(\phi_{cl}) \quad (3.74)$$

$$-\frac{1}{4\pi^2} \int_{m_f}^{M_f} M_f (M_f^2 - 1) \left(\psi^{(0)} (|M_f| - 1) + \psi^{(0)} (|M_f| + 2) \right) dM_f \sim -\frac{g^4}{8\pi^2} \phi_{cl}^4 \log(\phi_{cl}) \quad (3.75)$$

These asymptotic behavior imply that the potential remains bounded for $\lambda_4 > 4g^2$. Note that this constraint is same as that in flat space [34]. It is taken care of in the following numerical analysis where $\lambda_4 = 0.8$ so that $g < 0.447$. λ_3 is set to zero.

The full potential including the finite temperature piece is

$$V_{eff} = V_{eff}^0 - \frac{3}{2\pi\beta} \sum_{n=1}^{\infty} \frac{1}{n} \frac{e^{-n\beta(\frac{3}{2} + \sqrt{\frac{9}{4} + M_s^2})}}{|1 - e^{-n\beta}|^3} + \frac{6}{\pi\beta} \sum_{n=1}^{\infty} \frac{(-1)^n}{n} \frac{e^{-n\beta(\frac{3}{2} + |M_f|)}}{|1 - e^{-n\beta}|^3}. \quad (3.76)$$

At zero temperature Figure 6 shows the phases on the m_f - g plane for positive and negative values of m_s^2 and related potential plots. In Figure 6a there is a transition across the boundary separating *II* and *III*. This is same as in the case of AdS_2 . The potential plots corresponding to regions in Figure 6a are similar to those in Figure 4 for the case of AdS_2 .

In Figure 6b, we have plotted the regions *i-iv* corresponding to the nature of the potentials (shown on extreme right) on the left of the origin $\phi_{cl} = 0$. The minimum right of the origin and a maximum at the origin (as per the renormalization condition (3.73)) always exist for negative values of m_s^2 . The dashed line is the phase boundary. In regions *ii* and *iii* there are two minima left of the origin.

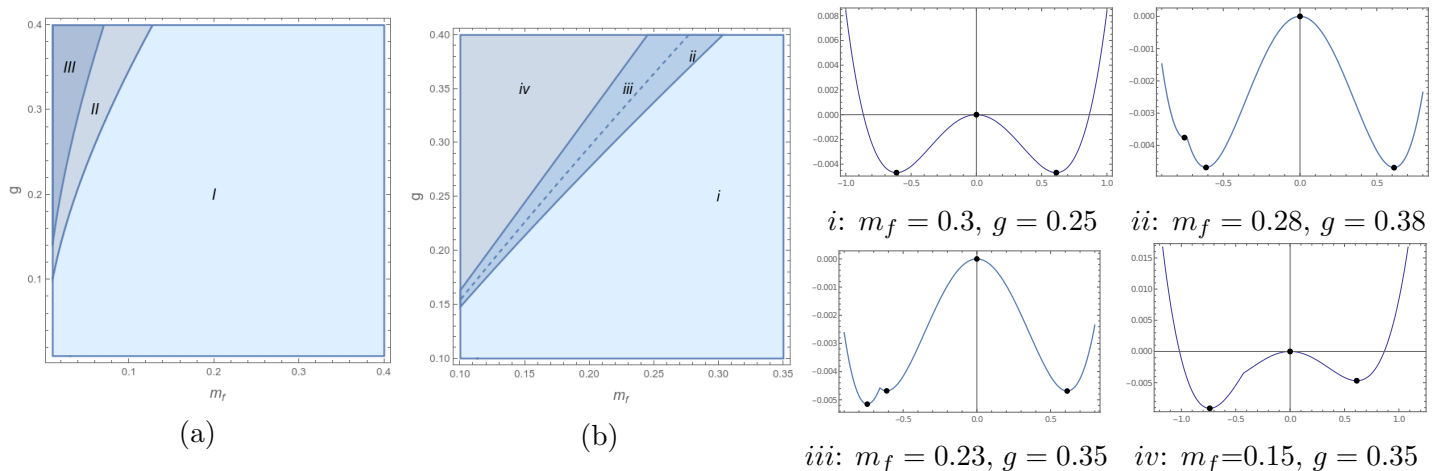


Figure 6: Phases at zero temperature in the m_f - g plane for (a) $m_s^2 = 0.05$ and (b) $m_s^2 = -0.05$. Representative potentials *i – iv* corresponding to regions in (b) are on extreme right. Black dots on the potential plots are the extrema.

The presence of the cusp at $m_f + g\phi_{cl} = 0$ poses a complication in the analysis of phases at finite temperature. We thus set $m_f = 0.8, g = 0.1$ so that the cusp falls on the left of the interesting region. This (m_f, g) point corresponds to a point in region *I* at zero temperature in Figure 6a. The phase plots and the corresponding potentials at finite temperature are given in Figure 7. We see the following features.

1. There is always a root of the saddle point equation at the left of the origin which is a minimum and this is the only one for all positive m_s^2 . This is region *A* in Figure 7a.
2. For $m_s^2 < 0$ which at low temperatures in region *B* we have two additional extrema, a maximum and a minimum. These extrema vanish at high temperatures as in theories of scalars [15] where the the $O(N)$ symmetry gets restored.
3. Another set of new extrema appear for lower values of masses. This is in region *D* in Figure 7a. This feature is also similar to that of the scalars. The differences in this case is that the potential is asymmetric about $\phi_{cl} = 0$ and there is a cusp (which are not shown in the potential plots). The additional extrema in region *D* survive in region *C* which vanish as one moves into region *A*.
4. Figure 7b shows the contours for extrema at various values of ϕ_{cl} . Two contours intersect when two extrema exist simultaneously. The boundaries of regions *C* and *D* of Figure 7a envelopes the regions of the contour intersection giving rise to additional extrema.
5. We find that the extreme left minimum remains the global minimum for all values of masses and temperatures.

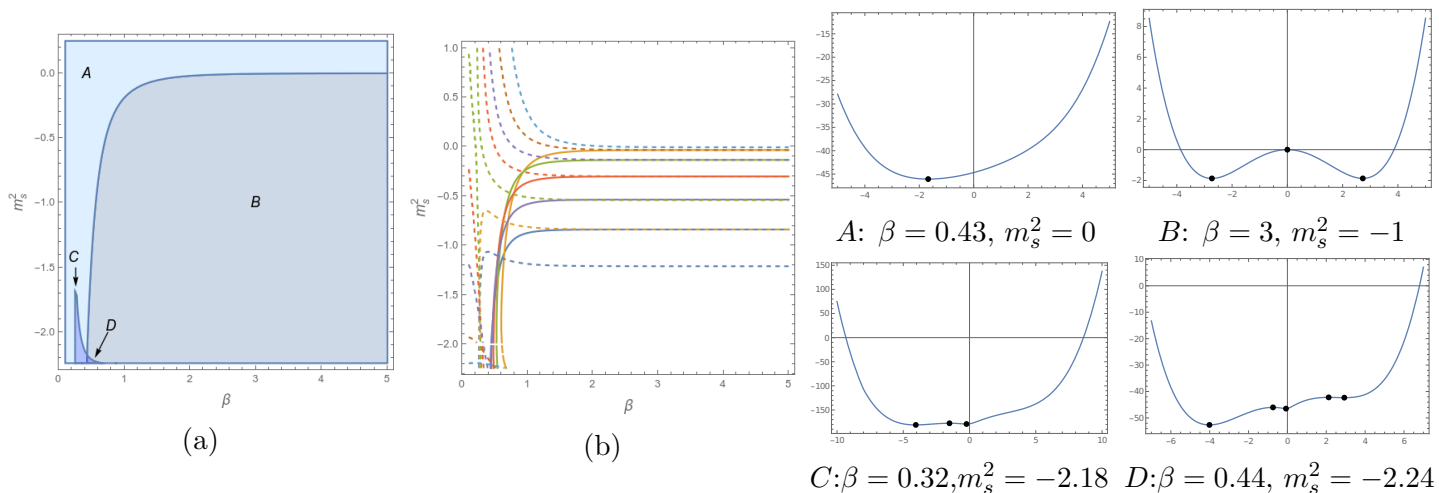


Figure 7: (a): Phases for $m_f = 0.8$ and $g = 0.1$ in the β - m_s^2 plane and representative potentials *A-D* on extreme right. Black dots on the potential plots are the extrema. (b): Contours for the extrema at various values of ϕ_{cl} . The solid lines range from $\phi_{cl} = 2.5$ to 0.5 and the dashed lines are for $\phi_{cl} = -3$ to -0.2 .

3.2 Gross-Neveu model

In this section we study the phases of massive Gross-Neveu model. The Euclidean theory is given by

$$\mathcal{L} = \bar{\psi}^i (\not{D} + m_f) \psi^i + \frac{g}{2N} (\bar{\psi}^i \psi^i)^2, \quad i = 1, \dots, N \quad (3.77)$$

The large N computation proceeds similar to that in flat space. We thus review the essential ingredients. It is convenient to introduce an auxiliary field $\sigma(x)$ and define

$$\begin{aligned}\mathcal{L}' &= \mathcal{L} - \frac{N}{2g} \left(\sigma(x) - \frac{g}{N} \bar{\psi}^i \psi^i \right)^2 \\ &= \bar{\psi}^i (\not{D} + m_f + \sigma(x)) \psi^i - \frac{N}{2g} \sigma^2(x)\end{aligned}\tag{3.78}$$

Imposing the σ equation of motion $\sigma = (g/N) \bar{\psi}^i \psi^i$ one recovers the original theory (3.77) with four fermion interaction. In (3.78) the fermions being quadratic, can now be integrated over

$$\begin{aligned}Z &= \int \mathcal{D}\sigma \mathcal{D}\bar{\psi}^i \mathcal{D}\psi^i \exp \left(- \int d^{d+1}x \sqrt{g} \mathcal{L}' \right) \\ &= \int \mathcal{D}\sigma [\det (\not{D} + m_f + \sigma(x))]^N \exp \left(\frac{N}{2g} \sigma^2(x) \right).\end{aligned}\tag{3.79}$$

Writing $\sigma(x) = \sigma_{cl} + \delta\sigma(x)$, one arrives at the following effective potential as a function of σ_{cl} at the leading order in $1/N$

$$\frac{V_{eff}}{N} = -\frac{\sigma_{cl}^2}{2g} - \text{tr} \log (\not{D} + m_f + \sigma_{cl})\tag{3.80}$$

The saddle point equation is

$$\frac{1}{N} \frac{\partial V_{eff}}{\partial \sigma_{cl}} = -\frac{\sigma_{cl}}{g} - \text{tr} \left[\frac{1}{\not{D} + m_f + \sigma_{cl}} \right]\tag{3.81}$$

We now analyze the potential (3.80) for $m_f, g > 0$. The extrema of the potential is determined by the real roots of the saddle point equation (3.81). The changes in the phase plots at finite temperature are discussed further.

3.2.1 AdS₃

For AdS₃, the potential and the saddle point equations at zero temperature are respectively

$$\frac{V_{eff}^0}{N} = -\frac{\sigma_{cl}^2}{2g} + \frac{1}{2\pi} \left(\frac{1}{3} |m_f + \sigma_{cl}|^3 - \frac{1}{4} |m_f + \sigma_{cl}| \right)\tag{3.82}$$

$$\frac{1}{N} \frac{\partial V_{eff}^0}{\partial \sigma_{cl}} = -\frac{\sigma_{cl}}{g} + \frac{1}{2\pi} \text{sgn}(m_f + \sigma_{cl}) \left((m_f + \sigma_{cl})^2 - \frac{1}{4} \right) = 0.\tag{3.83}$$

We summarize below the essential features of the potential. The saddle point equation being quadratic, has a maximum of two roots.

1. For $\text{sgn}(m_f + \sigma_{cl}) = +1$ i.e. for $\sigma_{cl} > -m_f$, there are two roots when $m_f > g/(8\pi)$ corresponding to a minimum and a maximum of the potential. On the $(m_f - g)$ plane this region is B in Figure 8. Otherwise in region A there is only one minimum. No roots exist when $\pi^2/g^2 - 2\pi m_f/g + 1/4 < 0$ (region C). The solid lines in Figure 8 are the boundaries of these regions at zero temperature. At the boundary separating regions B and C the maximum and the minimum in region B coincide.
2. For $\text{sgn}(m_f + \sigma_{cl}) = -1$ i.e. for $\sigma_{cl} < -m_f$, there exists one root corresponding to a minimum of the potential for all values of m_f and g .
3. The minimum on the left always remains lower than that of the right, whenever the right minimum exists. In other words, there is no first order phase transition. This has been checked numerically.
4. For $m_f = 0$ the potential is symmetric under $\sigma_{cl} \rightarrow -\sigma_{cl}$. This originates from the discrete chiral symmetry for $m_f = 0$, $\psi \rightarrow \gamma^5 \psi$ exactly as in flat space case. However the deviation from the flat space appears in the last term on the r.h.s in equation (3.82) as also in the Yukawa theory in AdS₃ discussed earlier. This term results in the potential being non-differentiable at $m_f + \sigma_{cl} = 0$. Putting back factors of the AdS radius L it is easy to see that the term can be ignored as compared to the first two terms in r.h.s of equation (3.82) as $L \rightarrow \infty$. Thus the maximum that appears in the flat space case at $\sigma_{cl} = 0$ for $m_f = 0$ is replaced by a cusp.

At finite temperature,

$$\frac{V_{eff}}{N} = \frac{V_{eff}^0}{N} - \frac{4}{\pi\beta} \sum_{n=1}^{\infty} \frac{(-1)^n e^{-n\beta(1+|m_f+\sigma_{cl}|)}}{n |1 - e^{-n\beta}|^2}. \quad (3.84)$$

The corresponding boundary that separates regions A and B at zero temperature is now given by

$$\left. \frac{1}{N} \frac{\partial V_{eff}}{\partial \sigma_{cl}} \right|_{\sigma_{cl}+m_f=0+} = \frac{m_f}{g} - \frac{1}{8\pi} + \frac{4}{\pi} \sum_{n=1}^{\infty} \frac{(-1)^n e^{-n\beta}}{|1 - e^{-n\beta}|^2} = 0. \quad (3.85)$$

This boundary is shown as the dashed straight line in Figure 8. The finite temperature contribution decreases the slope and as a result the region A now expands to include the region $A1$. The region where no right extremum exists shrinks at finite temperature to the region enclosed by the dashed curve. It is known that in flat space, at high temperatures (for tree-level, $m_f = 0$) the discrete chiral symmetry is restored [40, 41]. However we find that in AdS₃ it remains broken for all temperatures.

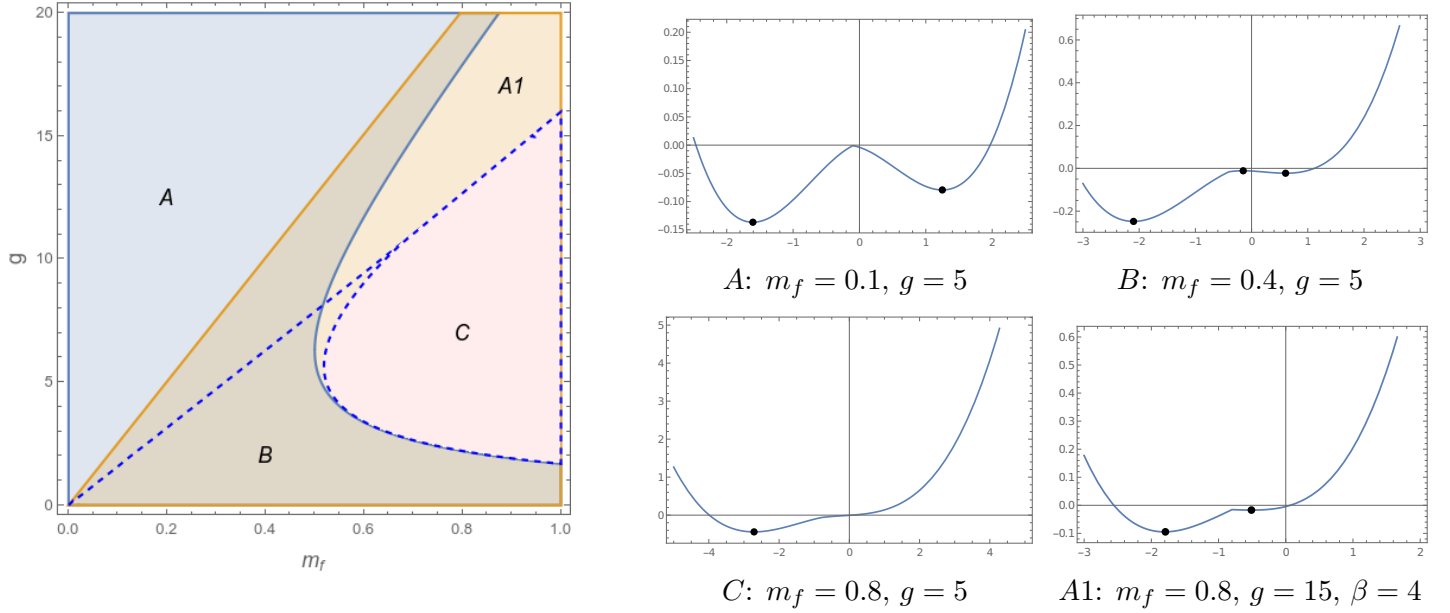


Figure 8: Regions (left) corresponding to various representative potentials (right). The solid lines correspond to boundaries at zero temperature and the dashed lines for $\beta = 4$ and $n = 10$. Black dots on the potential plots are the extrema.

3.2.2 AdS₂

The zero temperature trace is UV divergent and can be regularized using dimensional regularization. We expand about $d = 1$ with $\epsilon = 1 - d$. The expression for the zero temperature trace is given in (3.67). In terms of Feynman diagrams, the UV divergences arise from the two-point and the one-point diagrams. We thus use the following structure of the counterterms

$$\sigma_{cl} \delta\lambda_1 + \frac{1}{2}\sigma_{cl}^2 \delta\left(\frac{1}{g}\right)$$

with renormalization conditions

$$\left. \frac{1}{N} \frac{\partial V_{eff}^0}{\partial \sigma_{cl}} \right|_{\sigma_{cl}=0} = 0 \quad \left. \frac{1}{N} \frac{\partial^2 V_{eff}^0}{\partial \sigma_{cl}^2} \right|_{\sigma_{cl}=0} = -\frac{1}{g}. \quad (3.86)$$

These give the following zero temperature effective potential

$$V_{eff}^0 = -\frac{\sigma_{cl}^2}{2g} + \frac{1}{2\pi} \int_{m_f}^{M_f} M_f \left(\psi^{(0)}(|M_f|) + \psi^{(0)}(|M_f| + 1) \right) dM_f - \sigma_{cl} \left[\frac{m_f}{2\pi} \left(\psi^{(0)}(m_f) + \psi^{(0)}(m_f + 1) \right) \right]$$

$$- \frac{\sigma_{cl}^2}{4\pi} \left[\left(\psi^{(0)}(m_f) + \psi^{(0)}(m_f + 1) \right) + m_f \left(\psi^{(1)}(m_f) + \psi^{(1)}(m_f + 1) \right) \right] \quad (3.87)$$

To see the large σ_{cl} behaviour we expand the integrand in (3.87). $\psi^{(0)}(\sigma_{cl})$ for large σ_{cl} behaves as $\log(\sigma_{cl})$. Thus after integration the leading positive term is $\sigma_{cl}^2 \log(\sigma_{cl})$. This is behaviour of the large N correction in flat space in two dimensions. In three dimensions the leading term is σ_{cl}^3 . Since $\log(\sigma_{cl})$ grows slowly than σ_{cl} , we need to choose somewhat larger values of g in the numerics so as to get the extrema of the potential within a small range of σ_{cl} . A further point to note is that since we have set the renormalization condition at $\sigma_{cl} = 0$, m_f cannot be taken to be zero due to infrared divergences. One needs to set the renormalization conditions (3.86) at some nonzero value, $\sigma_{cl} = \sigma_0$. In this case, because of the discrete chiral and $\sigma \rightarrow -\sigma$ symmetries for $m_f = 0$, the potential is symmetric about $\sigma_{cl} = 0$ with two minima as in flat space. The discrete chiral symmetry (of the massless theory) is spontaneously broken.

Returning back to the massive theory, the finite temperature effective potential is

$$\frac{V_{eff}}{N} = \frac{V_{eff}^0}{N} - \frac{2}{\beta} \sum_{n=1}^{\infty} \frac{(-1)^n e^{-n\beta(\frac{1}{2}+|M_f|)}}{n |1 - e^{-n\beta}|}. \quad (3.88)$$

We now summarize the essential features of the potential below.

1. At zero temperature there are two minima for all values of (m_f, g) coming from the two branches of the potential $\sigma_{cl} + m_f > 0$ and $\sigma_{cl} + m_f < 0$. The left minimum is lower than the right in the (m_f, g) plane. In the left branch we only have the minimum. The renormalization condition (3.86) imply that at $\sigma_{cl} = 0$ there is a maximum for all positive values of g . This is unlike the case of AdS₃ where there are additional B and C regions. Note that the maximum always comes right of the cusp because $m_f > 0$ and the cusp is at $\sigma_{cl} + m_f = 0$. A plot of the potential at $T = 0$ is shown in Figure 9 (right).
2. The two minima remain at finite temperatures and the left minimum remains lower than the right. Figure 9a shows two regions A and B . In region A the maximum ceases to exist unlike that in region B . The dashed lines in the figure are the corresponding boundaries for $\beta = 3, 5$. Representative potential plots are shown in the right of Figure 9a. For high values of g a new minimum appears from the right branch ($m_f + \sigma_{cl} > 0$) shown in the figure labelled as R .

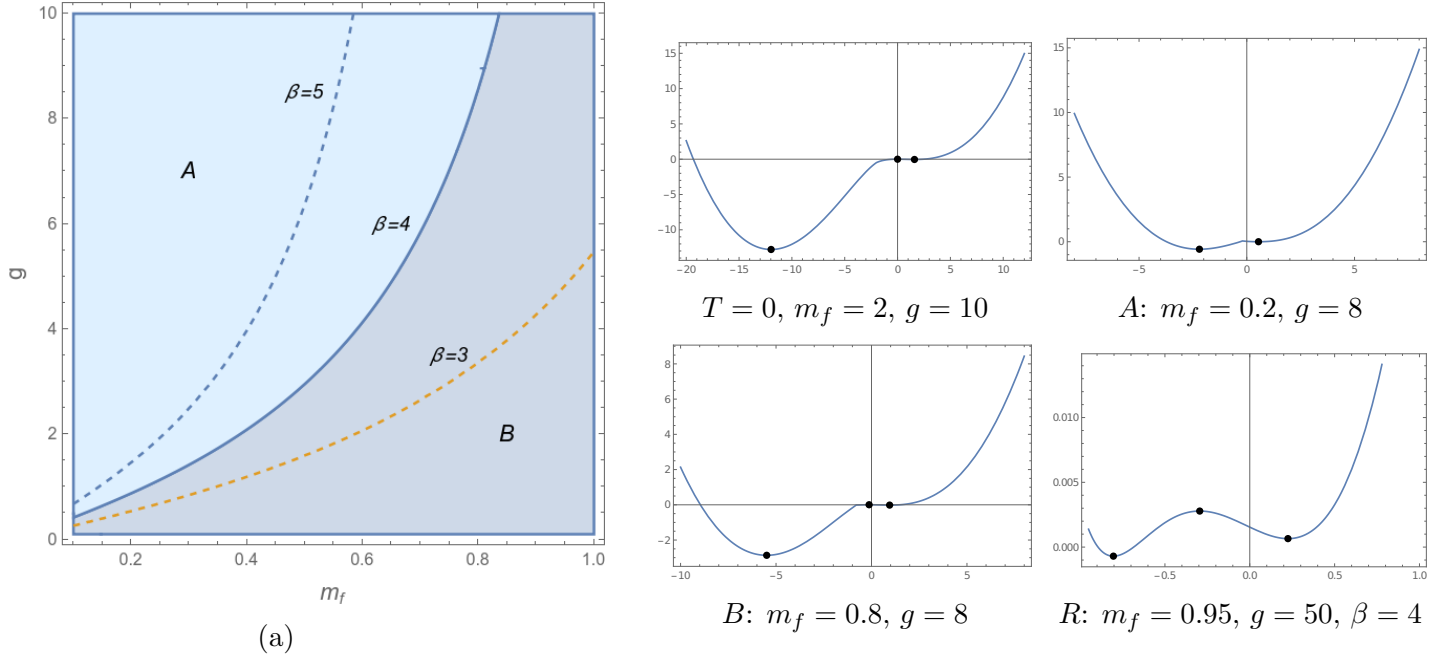


Figure 9: Regions in (m_f, g) space (left) and some potential plots (right). The solid boundary separates the shaded regions A and B for $\beta = 4$. The corresponding boundaries for $\beta = 3, 5$ are shown as dashed lines. Black dots on the potential plots are the extrema.

3.2.3 AdS₄

In four dimensions, since the four-fermion theory is not renormalizable, we need to add additional scalar interactions. To see this, we expand the zero temperature fermion trace about $d = 3$ with $\epsilon = 3 - d$ as in (3.72). One to four point functions in σ_{cl} are UV divergent. The counterterms have the following form

$$\sigma_{cl} \delta\lambda_1 + \frac{1}{2}\sigma_{cl}^2 \delta\left(\frac{1}{g}\right) + \frac{1}{3!}\sigma_{cl}^3 \delta\lambda_3 + \frac{1}{4!}\sigma_{cl}^4 \delta\lambda_4.$$

We use the renormalization scheme as in the previous section for AdS₂, with the following renormalization conditions at $\sigma_{cl} = 0$

$$\frac{1}{N} \frac{\partial V_{eff}^0}{\partial \sigma_{cl}} = 0 \quad \frac{1}{N} \frac{\partial^2 V_{eff}^0}{\partial \sigma_{cl}^2} = -\frac{1}{g} \quad \frac{1}{N} \frac{\partial^3 V_{eff}^0}{\partial \sigma_{cl}^3} = \lambda_3 \quad \frac{1}{N} \frac{\partial^4 V_{eff}^0}{\partial \sigma_{cl}^4} = \lambda_4. \quad (3.89)$$

These give the following zero temperature effective potential

$$\begin{aligned}
V_{eff}^0 &= -\frac{\sigma_{cl}^2}{2g} + \lambda_3 \frac{\sigma_{cl}^3}{3!} + \lambda_4 \frac{\sigma_{cl}^4}{4!} - \int_{m_f}^{M_f} \frac{M_f(M_f^2 - 1)}{4\pi^2} \left(\psi^{(0)}(|M_f| - 1) + \psi^{(0)}(|M_f| + 2) \right) dM_f \\
&+ \frac{\sigma_{cl}^4}{4!} \left[\frac{3}{2\pi^2} \left(\psi^{(0)}(m_f - 1) + \psi^{(0)}(m_f + 2) \right) + \frac{9m_f}{2\pi^2} \left(\psi^{(1)}(m_f - 1) + \psi^{(1)}(m_f + 2) \right) \right. \\
&+ \left. \frac{3}{4\pi^2} (3m_f^2 - 1) \left(\psi^{(2)}(m_f - 1) + \psi^{(2)}(m_f + 2) \right) + \frac{(m_f^3 - m_f)}{4\pi^2} \left(\psi^{(3)}(m_f - 1) + \psi^{(3)}(m_f + 2) \right) \right] \\
&+ \frac{\sigma_{cl}^3}{3!} \left[\frac{3m_f}{2\pi^2} \left(\psi^{(0)}(m_f - 1) + \psi^{(0)}(m_f + 2) \right) + \frac{(3m_f^2 - 1)}{2\pi^2} \left(\psi^{(1)}(m_f - 1) + \psi^{(1)}(m_f + 2) \right) \right. \\
&+ \left. \frac{(m_f^3 - m_f)}{4\pi^2} \left(\psi^{(2)}(m_f - 1) + \psi^{(2)}(m_f + 2) \right) \right] \\
&+ \frac{\sigma_{cl}^2}{2!} \left[\frac{(3m_f^2 - 1)}{4\pi^2} \left(\psi^{(0)}(m_f - 1) + \psi^{(0)}(m_f + 2) \right) + \frac{(m_f^3 - m_f)}{4\pi^2} \left(\psi^{(1)}(m_f - 1) + \psi^{(1)}(m_f + 2) \right) \right] \\
&+ \sigma_{cl} \left[\frac{(m_f^3 - m_f)}{4\pi^2} \left(\psi^{(0)}(m_f - 1) + \psi^{(0)}(m_f + 2) \right) \right] \tag{3.90}
\end{aligned}$$

Note however that the the fermion trace in the first line of (3.90) gives the following leading behavior for large values of σ_{cl}

$$-\int_{m_f}^{M_f} \frac{M_f(M_f^2 - 1)}{4\pi^2} \left(\psi^{(0)}(|M_f| - 1) + \psi^{(0)}(|M_f| + 2) \right) dM_f \sim -\sigma_{cl}^4 \log(\sigma_{cl}) \tag{3.91}$$

which makes the potential unbounded below. We thus also add the kinetic term for the σ field and write the modified theory as

$$\mathcal{L}' = \bar{\psi}^i (\not{D} + m_f + g\sigma) \psi^i + \frac{1}{2}(\partial_\mu \sigma)^2 + \frac{1}{2}m_s^2 \sigma^2 + \lambda_3 \frac{\sigma^3}{3!} + \lambda_4 \frac{\sigma^4}{4!} \tag{3.92}$$

which is known as the Gross-Neveu-Yukawa model [42]. To study the large N behavior we re-scale $\sigma \rightarrow \sqrt{N}\sigma$, $g \rightarrow g/\sqrt{N}$, $\lambda_3 \rightarrow \lambda_3/\sqrt{N}$, $\lambda_4 \rightarrow \lambda_4/N$. Then writing $\sigma = \sigma_{cl} + \delta\sigma$ and integrating over the fluctuations $\delta\sigma$ gives

$$\frac{V_{eff}^0}{N} = \frac{1}{2}m_s^2 \sigma_{cl}^2 + \frac{\lambda_3}{3!} \sigma_{cl}^3 + \frac{\lambda_4}{4!} \sigma_{cl}^4 - \frac{1}{2\mathcal{V}_{d+1}} \int_{M_s^2}^{\infty} \text{tr} \left[\frac{1}{-\square_E + M_s^2} \right] dM_s^2 - \frac{1}{\mathcal{V}_{d+1}} \int_0^{M_f} \text{tr} \left[\frac{1}{\not{D} + M_f} \right] dM_f$$

+ counterterms

with $M_s^2 = m_s^2 + \lambda_3 \sigma_{cl} + \lambda_4 \sigma_{cl}^2/2$ and $M_f = m_f + g \sigma_{cl}$, which is essentially same as the Yukawa model studied in section 3.1.3.

4 Discussion

In this paper we have explored the phases of Yukawa theories and the Gross-Neveu models in AdS_{d+1} spaces for $d = 1, 2, 3$ at both zero and finite temperature. The analysis leads to qualitative features which at certain places deviate from those in flat space. This is in line with the expectation that the infrared behaviour of the theories is different from those in flat space. The paper begins with the description of a method, based on the premise that the generalized eigenfunctions of the Laplacian operator in Euclidean AdS obey the desired periodicities under the required thermal identification, for computing the one-loop partition function $Z^{(1)}$ for fermions. Our method, as described in this paper, reproduces the partition function results already known in literature. This computation is also shown to generalize to thermal AdS spaces of arbitrary dimensions.

It was observed from our previous analysis of scalars in [15] that, while the zero temperature contribution to the trace is proportional to the divergent volume of AdS_{d+1} , the finite temperature contribution is not. We have thus used the regularized volumes as has been discussed in [15]. The ultraviolet behavior of the theories being the same as that of flat space, we used dimensional regularization and renormalized perturbation theory to renormalize the divergent effective potentials. An alternate scheme, which is similar to the minimal subtraction scheme, has also been discussed for the Yukawa theories in appendix B.2.

We first performed the analysis for the Yukawa theories wherein we studied the phases of these field theories in the corresponding parameter spaces first at zero temperature and then at finite temperature. For all cases at zero temperature we found a phase boundary where two minima exchange dominance. This feature was also observed at finite temperature for AdS_2 and AdS_3 . We next studied the massive Gross-Neveu models. The Gross-Neveu Yukawa model was studied for $d = 3$. In the large N limit with proper re-scaling of the parameters by N , the potential in this case reduces to that of the Yukawa model in AdS_4 . For the Gross-Neveu models for $d = 1, 2$, the phases at zero temperature in the corresponding parameter space and the subsequent changes in them at finite temperature were discussed. We found that in the large N limit, unlike in flat space where the discrete chiral symmetry gets restored beyond a certain temperature [37]-[41], the discrete chiral symmetry appearing in the $m_f = 0$ limit remains broken at all temperatures both for two and three dimensions.

This study of the one-loop partition functions paves way for future research in various directions.

The analysis can be extended to other theories involving fermions such as those with continuous chiral symmetries and with vector fields in thermal AdS spaces. Work along these lines is in progress. Till now our analysis has been limited to spaces where the background space is a fixed thermal AdS. A more interesting and involved setup is to consider asymptotically AdS black hole geometry. At high temperatures it is known that the black hole is a more stable background through the Hawking-Page transition when one considers the gravitational fluctuations. Another possible promising direction is to compute non-perturbative effective potentials in the flat space limit using techniques implemented in recent studies on flat space S-Matrix as noted in the opening paragraph of the introduction.

Acknowledgements :

Astha Kakkar acknowledges the support of Department of Science and Technology (DST), Ministry of Science and Technology, Government of India, for the DST INSPIRE Fellowship with the INSPIRE Fellowship Registration Number: IF180721. S.S. thanks the University Grants Commission (UGC), and DST, New Delhi, India, for providing special assistance and infrastructural support to the Department of Physics, Vidyasagar University, through the SAP and FIST program respectively.

A Some details of zero temperature computation

A.1 Derivation of the measure $\mu(\lambda)$

Consider the integrals [43]

$$\int_0^\infty dy y^\alpha K_{i\lambda-\frac{1}{2}}(y)K_{-i\lambda'-\frac{1}{2}}(y) = \frac{2^{\alpha-2}}{\Gamma(1+\alpha)} \left[\Gamma\left(\frac{\alpha}{2} + \frac{i}{2}(\lambda - \lambda')\right) \Gamma\left(\frac{\alpha+2}{2} - \frac{i}{2}(\lambda - \lambda')\right) \Gamma\left(\frac{\alpha+1}{2} + \frac{i}{2}(\lambda + \lambda')\right) \Gamma\left(\frac{\alpha+1}{2} - \frac{i}{2}(\lambda + \lambda')\right) \right] \quad (\text{A.93})$$

$$\int_0^\infty dy y^\alpha K_{i\lambda+\frac{1}{2}}(y)K_{-i\lambda'+\frac{1}{2}}(y) = \frac{2^{\alpha-2}}{\Gamma(1+\alpha)} \left[\Gamma\left(\frac{\alpha}{2} - \frac{i}{2}(\lambda - \lambda')\right) \Gamma\left(\frac{\alpha+2}{2} + \frac{i}{2}(\lambda - \lambda')\right) \Gamma\left(\frac{\alpha+1}{2} + \frac{i}{2}(\lambda + \lambda')\right) \Gamma\left(\frac{\alpha+1}{2} - \frac{i}{2}(\lambda + \lambda')\right) \right] \quad (\text{A.94})$$

Adding equations (A.93) and (A.94), the r.h.s is

$$\frac{2^{\alpha-2}}{\Gamma(\alpha)} \Gamma\left(\frac{\alpha+1}{2} + \frac{i}{2}(\lambda + \lambda')\right) \Gamma\left(\frac{\alpha+1}{2} - \frac{i}{2}(\lambda + \lambda')\right) \Gamma\left(\frac{\alpha}{2} + \frac{i}{2}(\lambda - \lambda')\right) \Gamma\left(\frac{\alpha}{2} - \frac{i}{2}(\lambda - \lambda')\right) \quad (\text{A.95})$$

We are interested in the limit $\alpha \rightarrow 0$. In this limit, for $\lambda \neq \lambda'$, the r.h.s $\rightarrow 0$ since

$$\Gamma(x) \sim \frac{1}{x} \quad \text{as } x \rightarrow 0. \quad (\text{A.96})$$

For $\lambda \rightarrow \lambda'$ we write the r.h.s (A.95) using (A.96)

$$\begin{aligned} \Gamma\left(\frac{1}{2} + i\lambda\right) \Gamma\left(\frac{1}{2} - i\lambda\right) \left[\frac{\alpha}{(\lambda - \lambda')^2 + \alpha^2} \right] &\sim \pi \delta(\lambda - \lambda') \Gamma\left(\frac{1}{2} + i\lambda\right) \Gamma\left(\frac{1}{2} - i\lambda\right) \\ &= \delta(\lambda - \lambda') / \mu(\lambda) \end{aligned} \quad (\text{A.97})$$

A.2 λ contour integral in (2.17)

The integrand:

$$f(\lambda) = \frac{1}{\lambda^2 + M_f^2} \frac{\Gamma\left(\frac{d+1}{2} + i\lambda\right) \Gamma\left(\frac{d+1}{2} - i\lambda\right)}{\Gamma\left(\frac{1}{2} + i\lambda\right) \Gamma\left(\frac{1}{2} - i\lambda\right)} \quad (\text{A.98})$$

In the upper half of the complex λ -plane the contributions from poles are as follows.

1. $\lambda = iM_f$ with $M_f > 0$ pole from $\frac{1}{\lambda^2 + M_f^2}$

$$[2\pi i \text{Res}f(\lambda)]_1 = \frac{1}{M_f} \Gamma\left(\frac{d+1}{2} + M_f\right) \Gamma\left(\frac{d+1}{2} - M_f\right) \cos(\pi M_f) \quad (\text{A.99})$$

2. The gamma function $\Gamma\left(\frac{d+1}{2} + i\lambda\right)$ has poles for

$$\frac{d+1}{2} + i\lambda = -n \quad n = 0, 1, 2, \dots \quad \text{or} \quad \lambda = i\left(n + \frac{d+1}{2}\right).$$

Using $\text{Res}\Gamma(iz) = (-i)(-1)^n/n!$
 $z=in$

$$\begin{aligned} [2\pi i \text{Res}f(\lambda)]_2 &= 2\pi \sum_{n=0}^{\infty} \left[\frac{1}{M_f^2 - ((d+1)/2 + n)^2} \right] \frac{(-1)^n}{n!} \frac{\Gamma(n + (d+1))}{\Gamma(1/2 + (n + \frac{d+1}{2})) \Gamma(1/2 - (n + \frac{d+1}{2}))} \\ &= -\frac{1}{M_f} \Gamma\left(\frac{d+1}{2} + M_f\right) \Gamma\left(\frac{d+1}{2} - M_f\right) \sin(\pi M_f) \cot(\pi(d+1)/2) \end{aligned} \quad (\text{A.100})$$

Similar computation can be done for $M_f < 0$.

Thus

$$(\text{A.99}) + (\text{A.100}) = \frac{1}{M_f} \frac{\pi \Gamma((d+1)/2 + |M_f|)}{\Gamma(1/2 - d/2 + |M_f|) \sin(\pi(d+1)/2)} \quad (\text{A.101})$$

Putting in the other factors in (2.17) and using the identity

$$\Gamma(1/2 - d/2) \Gamma(1/2 + d/2) = \frac{\pi}{\sin(\pi(d+1)/2)}$$

gives the final expression (2.18).

A.3 An alternate computation of trace (2.15)

In this appendix we perform an alternate computation of the trace (2.15). The computation here differs from that in the main text in the order of k and λ integrals. Here we first perform the λ integral. We begin from equation (2.15) for the case of odd d .

$$\text{tr} \left[\frac{1}{\not{D} + M_f} \right] = \int d^{d+1}x \sqrt{g} \int \frac{d^d k}{(2\pi)^d} \frac{1}{k^d} \int_{-\infty}^{\infty} \frac{d\lambda}{i\lambda + M_f} \mu(\lambda) \psi_{\vec{k},\lambda}^\dagger(\vec{x}, y) \psi_{\vec{k},\lambda}(\vec{x}, y) \quad (\text{A.102})$$

$$\begin{aligned} &= 2^{\frac{d-1}{2}} \int d^{d+1}x \sqrt{g} \int \frac{d^d k}{(2\pi)^d} \frac{1}{k^d} \int_{-\infty}^{\infty} \frac{d\lambda}{\lambda^2 + M_f^2} \mu(\lambda) M_f \times \\ &\times (ky)^{d+1} \left[K_{-i\lambda - \frac{1}{2}}(ky) K_{i\lambda - \frac{1}{2}}(ky) + K_{-i\lambda + \frac{1}{2}}(ky) K_{i\lambda + \frac{1}{2}}(ky) \right]. \quad (\text{A.103}) \end{aligned}$$

Noting that $\mu(\lambda)$ is an even function, the following has been used in going from (A.102) to (A.103)

$$\begin{aligned} \int_{-\infty}^{\infty} \frac{d\lambda}{i\lambda + M_f} \mu(\lambda) &= \int_0^{\infty} \frac{d\lambda}{i\lambda + M_f} \mu(\lambda) + \int_0^{\infty} \frac{d\lambda}{-i\lambda + M_f} \mu(\lambda) \\ &= M_f \int_0^{\infty} \frac{d\lambda}{\lambda^2 + M_f^2} 2\mu(\lambda) = M_f \int_{-\infty}^{\infty} \frac{d\lambda}{\lambda^2 + M_f^2} \mu(\lambda). \quad (\text{A.104}) \end{aligned}$$

We next use the following relation

$$K_{i\lambda \pm \frac{1}{2}}(ky) = \frac{\pi}{2} \frac{I_{-i\lambda \mp \frac{1}{2}}(ky) - I_{i\lambda \pm \frac{1}{2}}(ky)}{i \sinh(\pi(\lambda + \frac{i}{2}))} = \frac{\pi}{2} \frac{I_{i\lambda \pm \frac{1}{2}}(ky) - I_{-i\lambda \mp \frac{1}{2}}(ky)}{\cosh(\pi\lambda)}. \quad (\text{A.105})$$

Therefore

$$K_{-i\lambda \pm \frac{1}{2}}(ky) K_{i\lambda \pm \frac{1}{2}}(ky) = \frac{\pi}{2} \frac{K_{-i\lambda \pm \frac{1}{2}}(ky) I_{i\lambda \pm \frac{1}{2}}(ky) - K_{i\lambda \mp \frac{1}{2}}(ky) I_{-i\lambda \mp \frac{1}{2}}(ky)}{\cosh(\pi\lambda)} \quad (\text{A.106})$$

where we have used the even parity property of the Bessel function of the second kind in the second term of r.h.s. Next consider the following identities [43]

$$\int_0^{\infty} J_{\mu+\nu}(2z \sinh t) \cosh[(\mu - \nu)t] dt = \frac{1}{2} [I_\nu(z) K_\mu(z) + I_\mu(z) K_\nu(z)] \quad (\text{A.107})$$

$$\int_0^{\infty} J_{\mu+\nu}(2z \sinh t) \sinh[(\mu - \nu)t] dt = \frac{1}{2} [I_\nu(z) K_\mu(z) - I_\mu(z) K_\nu(z)]. \quad (\text{A.108})$$

Adding equations (A.107) and (A.108)

$$\int_0^\infty J_{\mu+\nu}(2z \sinh t) \exp((\mu - \nu)t) dt = I_\nu(z) K_\mu(z). \quad (\text{A.109})$$

Out of the four terms from (A.105), we get for the following term

$$\frac{\pi}{2} \frac{1}{\cosh(\pi\lambda)} [K_{-i\lambda-\frac{1}{2}}(ky) I_{i\lambda-\frac{1}{2}}(ky)] = \frac{\pi}{2} \frac{1}{\cosh(\pi\lambda)} \int_0^\infty J_{-1}(2z \sinh t) \exp[-2i\lambda t] \quad (\text{A.110})$$

Using the property for the Bessel functions $J_{-\mu}(z) = (-1)^\mu J_\mu(z)$ for $\mu \in \mathbb{Z}$, the λ integral in the trace (A.103) becomes

$$- \int_{-\infty}^\infty \frac{d\lambda \mu(\lambda) M_f \pi}{\lambda^2 + M_f^2} (\cosh \pi\lambda)^{-1} \int_0^\infty J_1(2ky \sinh t) \exp[-2i\lambda t] dt \quad (\text{A.111})$$

and performing the λ integral in the lower half plane with the pole at $\lambda = -iM_f$ with $M_f > 0$

$$- \int_0^\infty J_1(2ky \sinh t) \exp[-2M_f t] dt = -K_{\frac{1}{2}-M_f}(ky) I_{\frac{1}{2}+M_f}(ky) \quad (\text{A.112})$$

Next performing the x and the k integrals in (A.103) and considering also the case for $M_f < 0$ gives

$$\begin{aligned} & -2^{(d-1)/2} V_{d+1} \left(\frac{2\pi^{d/2}}{\Gamma(d/2)(2\pi)^d} \right) \times \\ & \text{sgn}(M_f) \frac{1}{2} \left[2^{d-1} \Gamma\left(1 + \frac{d}{2}\right) \Gamma\left(\left(\frac{1+d}{2}\right) + |M_f|\right) {}_2F_{1R}\left(\frac{2+d}{2}, \frac{1+d}{2} + |M_f|, \frac{3}{2} + |M_f|, 1\right) \right] \end{aligned} \quad (\text{A.113})$$

The above expression can be simplified using the following relations

$${}_2F_{1R}(a, b, c; 1) = \frac{\Gamma(c-b-a)}{\Gamma(c-a)\Gamma(c-b)} \quad \text{and} \quad \Gamma(1-d/2) = \frac{2^d \sqrt{\pi} \Gamma(1-d)}{\Gamma(\frac{1}{2} - \frac{d}{2})} \quad (\text{A.114})$$

This gives the first contribution to the trace as

$$2^{(d-1)/2} \times \frac{1}{2} \times \text{sgn}(M_f) \frac{V_{d+1}}{(4\pi)^{(d+1)/2}} \frac{\Gamma(\frac{d+1}{2} + |M_f|) \Gamma(\frac{1}{2} - \frac{d}{2})}{\Gamma(\frac{1}{2} - \frac{d}{2} + |M_f|)} \quad (\text{A.115})$$

We use similar transformations for the other three terms from (A.105) as well. We perform the λ integral in the appropriate half of the plane to get four equal contributions from the four terms. This

gives the final expression for trace given by the r.h.s of (2.18). The factor of $2^{\frac{d-1}{2}}$ in the equation (A.103) comes from the number of components of $\psi_{\pm}(ky)$ for odd d . For even d this factor needs to be replaced by $2^{\frac{d-2}{2}}$. The result in this case is

$$\text{tr} \left[\frac{1}{\not{D} + M} \right] = \text{sgn}(M_f) \frac{\mathcal{V}_{d+1} 2^{\frac{d}{2}}}{(4\pi)^{(d+1)/2}} \frac{\Gamma\left(\frac{d+1}{2} + |M_f|\right) \Gamma\left(\frac{1}{2} - \frac{d}{2}\right)}{\Gamma\left(\frac{1}{2} - \frac{d}{2} + |M_f|\right)} \quad (\text{A.116})$$

B Effective potentials

B.1 Yukawa theory on AdS₄

Effective potential for Yukawa theory on AdS₄ at zero temperature resulting from the renormalization conditions (3.73) is

$$\begin{aligned} V_{eff}^0 &= \frac{1}{2} m_s^2 \phi_{cl}^2 + \frac{\lambda_3}{3!} \phi_{cl}^3 + \frac{\lambda_4}{4!} \phi_{cl}^4 + \frac{1}{2} \int_{m_s^2}^{M_s^2} \left(\frac{2 + M_s^2}{16\pi^2} \right) \left(\psi^{(0)} \left(\nu(\phi_{cl}) - \frac{1}{2} \right) + \psi^{(0)} \left(\nu(\phi_{cl}) + \frac{3}{2} \right) \right) dM_s^2 \\ &- \frac{1}{4\pi^2} \int_{m_f}^{M_f} M_f (M_f^2 - 1) \left(\psi^{(0)} (|M_f| - 1) + \psi^{(0)} (|M_f| + 2) \right) dM_f \\ &+ \phi_{cl} \left[\frac{g (m_f^3 - m_f)}{4\pi^2} \left(\psi^{(0)} (m_f - 1) + \psi^{(0)} (m_f + 2) \right) \right. \\ &- \left. \frac{\lambda_3 (m_s^2 + 2)}{32\pi^2} \left(\psi^{(0)} \left(\sqrt{m_s^2 + \frac{9}{4}} - \frac{1}{2} \right) + \psi^{(0)} \left(\sqrt{m_s^2 + \frac{9}{4}} + \frac{3}{2} \right) \right) \right] \\ &+ \frac{1}{2} \phi_{cl}^2 \left[\frac{g^2 (3m_f^2 - 1)}{4\pi^2} \left(\psi^{(0)} (m_f - 1) + \psi^{(0)} (m_f + 2) \right) + \frac{g^2 (m_f^3 - m_f)}{4\pi^2} \left(\psi^{(1)} (m_f - 1) + \psi^{(1)} (m_f + 2) \right) \right. \\ &- \frac{\lambda_3}{32\pi^2} \left(\lambda_3 \left(\psi^{(0)} \left(\sqrt{m_s^2 + \frac{9}{4}} - \frac{1}{2} \right) + \psi^{(0)} \left(\sqrt{m_s^2 + \frac{9}{4}} + \frac{3}{2} \right) \right) \right. \\ &+ \left. \left. \lambda_3 (m_s^2 + 2) \left(\frac{\psi^{(1)} \left(\sqrt{m_s^2 + \frac{9}{4}} - \frac{1}{2} \right)}{2\sqrt{m_s^2 + \frac{9}{4}}} + \frac{\psi^{(1)} \left(\sqrt{m_s^2 + \frac{9}{4}} + \frac{3}{2} \right)}{2\sqrt{m_s^2 + \frac{9}{4}}} \right) \right) \right. \\ &- \left. \left. \frac{\lambda_4}{32\pi^2} \left((m_s^2 + 2) \left(\psi^{(0)} \left(\sqrt{m_s^2 + \frac{9}{4}} - \frac{1}{2} \right) + \psi^{(0)} \left(\sqrt{m_s^2 + \frac{9}{4}} + \frac{3}{2} \right) \right) \right) \right) \right] \\ &+ \frac{1}{3!} \phi_{cl}^3 \left[\frac{3g^3 m_f (\psi^{(0)} (m_f - 1) + \psi^{(0)} (m_f + 2))}{2\pi^2} + \frac{g^3 (3m_f^2 - 1) (\psi^{(1)} (m_f - 1) + \psi^{(1)} (m_f + 2))}{2\pi^2} \right. \\ &+ \left. \frac{g^3 (m_f^3 - m_f) (\psi^{(2)} (m_f - 1) + \psi^{(2)} (m_f + 2))}{4\pi^2} \right] \end{aligned}$$

$$\begin{aligned}
& - \frac{\lambda_4}{16\pi^2} \left(\lambda_3 \left(\psi^{(0)} \left(\sqrt{m_s^2 + \frac{9}{4}} - \frac{1}{2} \right) + \psi^{(0)} \left(\sqrt{m_s^2 + \frac{9}{4}} + \frac{3}{2} \right) \right) \right. \\
& + \lambda_3(m_s^2 + 2) \left(\frac{\psi^{(1)} \left(\sqrt{m_s^2 + \frac{9}{4}} - \frac{1}{2} \right)}{2\sqrt{m_s^2 + \frac{9}{4}}} + \frac{\psi^{(1)} \left(\sqrt{m_s^2 + \frac{9}{4}} + \frac{3}{2} \right)}{2\sqrt{m_s^2 + \frac{9}{4}}} \right) \\
& - \frac{\lambda_3}{32\pi^2} \left(\lambda_4 \left(\psi^{(0)} \left(\sqrt{m_s^2 + \frac{9}{4}} - \frac{1}{2} \right) + \psi^{(0)} \left(\sqrt{m_s^2 + \frac{9}{4}} + \frac{3}{2} \right) \right) \right. \\
& + 2\lambda_3^2 \left(\frac{\psi^{(1)} \left(\sqrt{m_s^2 + \frac{9}{4}} - \frac{1}{2} \right)}{2\sqrt{m_s^2 + \frac{9}{4}}} + \frac{\psi^{(1)} \left(\sqrt{m_s^2 + \frac{9}{4}} + \frac{3}{2} \right)}{2\sqrt{m_s^2 + \frac{9}{4}}} \right) \\
& + (m_s^2 + 2) \left(\frac{\lambda_4 \psi^{(1)} \left(\sqrt{m_s^2 + \frac{9}{4}} - \frac{1}{2} \right)}{2\sqrt{m_s^2 + \frac{9}{4}}} - \frac{\lambda_3^2 \psi^{(1)} \left(\sqrt{m_s^2 + \frac{9}{4}} - \frac{1}{2} \right)}{4(m_s^2 + \frac{9}{4})^{3/2}} - \frac{\lambda_3^2 \psi^{(1)} \left(\sqrt{m_s^2 + \frac{9}{4}} + \frac{3}{2} \right)}{4(m_s^2 + \frac{9}{4})^{3/2}} \right. \\
& \left. \left. + \frac{\lambda_4 \psi^{(1)} \left(\sqrt{m_s^2 + \frac{9}{4}} + \frac{3}{2} \right)}{2\sqrt{m_s^2 + \frac{9}{4}}} + \frac{\lambda_3^2 \psi^{(2)} \left(\sqrt{m_s^2 + \frac{9}{4}} - \frac{1}{2} \right)}{4(m_s^2 + \frac{9}{4})} + \frac{\lambda_3^2 \psi^{(2)} \left(\sqrt{m_s^2 + \frac{9}{4}} + \frac{3}{2} \right)}{4(m_s^2 + \frac{9}{4})} \right) \right] \\
& + \frac{1}{4!} \phi_{cl}^4 \left[\frac{3g^4(\psi^{(0)}(m_f - 1) + \psi^{(0)}(m_f + 2))}{2\pi^2} + \frac{9g^4 m_f (\psi^{(1)}(m_f - 1) + \psi^{(1)}(m_f + 2))}{2\pi^2} \right. \\
& + \frac{3g^4(3m_f^2 - 1)(\psi^{(2)}(m_f - 1) + \psi^{(2)}(m_f + 2))}{4\pi^2} + \frac{g^4 m_f (m_f^2 - 1)(\psi^{(3)}(m_f - 1) + \psi^{(3)}(m_f + 2))}{4\pi^2} \\
& - \frac{3}{32\pi^2} \lambda_4 \left(\lambda_4 \left(\psi^{(0)} \left(\sqrt{m_s^2 + \frac{9}{4}} - \frac{1}{2} \right) + \psi^{(0)} \left(\sqrt{m_s^2 + \frac{9}{4}} + \frac{3}{2} \right) \right) \right. \\
& + 2\lambda_3^2 \left(\frac{\psi^{(1)} \left(\sqrt{m_s^2 + \frac{9}{4}} - \frac{1}{2} \right)}{2\sqrt{m_s^2 + \frac{9}{4}}} + \frac{\psi^{(1)} \left(\sqrt{m_s^2 + \frac{9}{4}} + \frac{3}{2} \right)}{2\sqrt{m_s^2 + \frac{9}{4}}} \right) \\
& + (m_s^2 + 2) \left(\frac{\lambda_4 \psi^{(1)} \left(\sqrt{m_s^2 + \frac{9}{4}} - \frac{1}{2} \right)}{2\sqrt{m_s^2 + \frac{9}{4}}} - \frac{\lambda_3^2 \psi^{(1)} \left(\sqrt{m_s^2 + \frac{9}{4}} - \frac{1}{2} \right)}{4(m_s^2 + \frac{9}{4})^{3/2}} + \frac{\lambda_4 \psi^{(1)} \left(\sqrt{m_s^2 + \frac{9}{4}} + \frac{3}{2} \right)}{2\sqrt{m_s^2 + \frac{9}{4}}} \right. \\
& \left. - \frac{\lambda_3^2 \psi^{(1)} \left(\sqrt{m_s^2 + \frac{9}{4}} + \frac{3}{2} \right)}{4(m_s^2 + \frac{9}{4})^{3/2}} + \frac{\lambda_3^2 \psi^{(2)} \left(\sqrt{m_s^2 + \frac{9}{4}} - \frac{1}{2} \right)}{4(m_s^2 + \frac{9}{4})} + \frac{\lambda_3^2 \psi^{(2)} \left(\sqrt{m_s^2 + \frac{9}{4}} + \frac{3}{2} \right)}{4(m_s^2 + \frac{9}{4})} \right) \right) \\
& - \frac{1}{32\pi^2} \lambda_3 \left(3\lambda_4 \left(\frac{\lambda_3 \psi^{(1)} \left(\sqrt{m_s^2 + \frac{9}{4}} - \frac{1}{2} \right)}{2\sqrt{m_s^2 + \frac{9}{4}}} + \frac{\lambda_3 \psi^{(1)} \left(\sqrt{m_s^2 + \frac{9}{4}} + \frac{3}{2} \right)}{2\sqrt{m_s^2 + \frac{9}{4}}} \right) \right)
\end{aligned}$$

$$\begin{aligned}
& + 3\lambda_3 \left(\frac{\lambda_4 \psi^{(1)} \left(\sqrt{m_s^2 + \frac{9}{4}} - \frac{1}{2} \right)}{2\sqrt{m_s^2 + \frac{9}{4}}} - \frac{\lambda_3^2 \psi^{(1)} \left(\sqrt{m_s^2 + \frac{9}{4}} - \frac{1}{2} \right)}{4 \left(m_s^2 + \frac{9}{4} \right)^{3/2}} - \frac{\lambda_3^2 \psi^{(1)} \left(\sqrt{m_s^2 + \frac{9}{4}} + \frac{3}{2} \right)}{4 \left(m_s^2 + \frac{9}{4} \right)^{3/2}} \right. \\
& + \frac{\lambda_4 \psi^{(1)} \left(\sqrt{m_s^2 + \frac{9}{4}} + \frac{3}{2} \right)}{2\sqrt{m_s^2 + \frac{9}{4}}} + \frac{\lambda_3^2 \psi^{(2)} \left(\sqrt{m_s^2 + \frac{9}{4}} - \frac{1}{2} \right)}{4 \left(m_s^2 + \frac{9}{4} \right)} + \frac{\lambda_3^2 \psi^{(2)} \left(\sqrt{m_s^2 + \frac{9}{4}} + \frac{3}{2} \right)}{4 \left(m_s^2 + \frac{9}{4} \right)} \left. \right) \\
& + \left(m_s^2 + 2 \right) \left(\frac{3\lambda_3^3 \psi^{(1)} \left(\sqrt{m_s^2 + \frac{9}{4}} - \frac{1}{2} \right)}{8 \left(m_s^2 + \frac{9}{4} \right)^{5/2}} - \frac{3\lambda_3 \lambda_4 \psi^{(1)} \left(\sqrt{m_s^2 + \frac{9}{4}} - \frac{1}{2} \right)}{4 \left(m_s^2 + \frac{9}{4} \right)^{3/2}} + \frac{3\lambda_3^3 \psi^{(1)} \left(\sqrt{m_s^2 + \frac{9}{4}} + \frac{3}{2} \right)}{8 \left(m_s^2 + \frac{9}{4} \right)^{5/2}} \right. \\
& - \frac{3\lambda_3 \lambda_4 \psi^{(1)} \left(\sqrt{m_s^2 + \frac{9}{4}} + \frac{3}{2} \right)}{4 \left(m_s^2 + \frac{9}{4} \right)^{3/2}} - \frac{3\lambda_3^3 \psi^{(2)} \left(\sqrt{m_s^2 + \frac{9}{4}} - \frac{1}{2} \right)}{8 \left(m_s^2 + \frac{9}{4} \right)^2} + \frac{3\lambda_3 \lambda_4 \psi^{(2)} \left(\sqrt{m_s^2 + \frac{9}{4}} - \frac{1}{2} \right)}{4 \left(m_s^2 + \frac{9}{4} \right)} \\
& - \frac{3\lambda_3^3 \psi^{(2)} \left(\sqrt{m_s^2 + \frac{9}{4}} + \frac{3}{2} \right)}{8 \left(m_s^2 + \frac{9}{4} \right)^2} + \frac{3\lambda_3 \lambda_4 \psi^{(2)} \left(\sqrt{m_s^2 + \frac{9}{4}} + \frac{3}{2} \right)}{4 \left(m_s^2 + \frac{9}{4} \right)} + \frac{\lambda_3^3 \psi^{(3)} \left(\sqrt{m_s^2 + \frac{9}{4}} - \frac{1}{2} \right)}{8 \left(m_s^2 + \frac{9}{4} \right)^{3/2}} \\
& \left. \left. + \frac{\lambda_3^3 \psi^{(3)} \left(\sqrt{m_s^2 + \frac{9}{4}} + \frac{3}{2} \right)}{8 \left(m_s^2 + \frac{9}{4} \right)^{3/2}} \right) \right] . \tag{B.117}
\end{aligned}$$

B.2 A different renormalization scheme

In this section we discuss an alternate renormalization scheme for the zero temperature partition function in the Yukawa theories. For simplicity we set the renormalized parameters $\lambda_1 = \lambda_3 = 0$ in (3.61) and rename $\lambda_4 = \lambda$.

AdS₂

We see that the coefficient of the UV divergent $1/\epsilon$ terms in (3.66) and in (3.67) adds up to $(M_s^2 - 2M_f^2)$ after the integral in (3.61), where M_s^2 and M_f are defined in (3.62). We can absorb these divergences into a single counterterm defined as

$$(M_s^2 - 2M_f^2) \delta$$

and using the renormalization condition

$$\left. \frac{\partial V_{eff}^0}{\partial \phi_{cl}} \right|_{\phi_{cl}=\phi_0} = 0. \tag{B.118}$$

$\phi_0 > 0$ is some undetermined constant and V_{eff}^0 is the zero temperature effective potential. The renormalization scheme used here is similar to that of the Minimal Subtraction (MS) scheme. We have

made a slight departure from the MS scheme, by imposing (B.118) because it is easier to track the extremum (at ϕ_0) in the numerics. This results in addition of finite terms proportional to $(M_s^2 - 2M_f^2)$.

The final expressions for the zero temperature effective potential is

$$\begin{aligned}
V_{eff}^0 &= \frac{1}{2}m_s^2\phi_{cl}^2 - m_s^2\frac{\phi_0}{\chi}(M_s^2 - 2M_f^2) + \frac{\lambda}{4!}\phi_{cl}^4 - \frac{\lambda}{3!}\frac{\phi_0^3}{\chi}(M_s^2 - 2M_f^2) \\
&- \frac{1}{4\pi} \left[\int_0^{M_s^2} \psi^{(0)} \left(\nu(\phi_{cl}) + \frac{1}{2} \right) dM_s^2 - \lambda \frac{\phi_0}{\chi} \psi^{(0)} \left(\nu(\phi_0) + \frac{1}{2} \right) (M_s^2 - 2M_f^2) \right] \\
&+ \frac{1}{2\pi} \left[\int_0^{M_f} M_f \left[\psi^{(0)}(|M_f|) + \psi^{(0)}(1 + |M_f|) \right] dM_f - g \frac{M_f}{\chi} \left[\psi^{(0)}(M_f) + \psi^{(0)}(1 + M_f) \right] \right]_{\phi_{cl}=\phi_0} (M_s^2 - 2M_f^2) \\
&+ \frac{1}{8\pi} \left[(M_s^2 \log(4\pi) - 2M_f^2 \log(2\pi)) - \frac{1}{\chi} (\lambda\phi_0 \log(4\pi) - 4M_f g \log(2\pi)) \right]_{\phi_{cl}=\phi_0} (M_s^2 - 2M_f^2) \quad (B.119)
\end{aligned}$$

where $\chi = \lambda\phi_0 - 4gM_f(\phi_0)$. In the above expression, pairs of terms written in a single line cancel for the l.h.s of (B.118).

AdS₄

These UV divergences in (3.61) can be cancelled by the following counterterms

$$(M_s^2 + 2M_f^2) \delta_1 + (M_s^4 - 4M_f^4) \delta_2. \quad (B.120)$$

along with the renormalization conditions,

$$\left. \frac{\partial V_{eff}^0}{\partial \phi_{cl}} \right|_{\phi_{cl}=\phi_0} = 0 \quad \left. \frac{\partial^2 V_{eff}^0}{\partial \phi_{cl}^2} \right|_{\phi_{cl}=\phi_0} = m_s^2. \quad (B.121)$$

These conditions which imply that the extremum at ϕ_0 is a minimum or maximum depending on the sign of m_s^2 give the following counterterms.

$$\delta_1 = \frac{1}{16\pi^2} \left[\frac{y_1 z_2 - y_2 z_1}{x_1 y_2 - x_2 y_1} \right] \quad ; \quad \delta_2 = \frac{1}{64\pi^2} \left[\frac{x_1 z_2 - x_2 z_1}{x_2 y_1 - x_1 y_2} \right] \quad (B.122)$$

where

$$x_1 = \frac{1}{16\pi^2}(\lambda\phi_0 + 4gM_f) \quad ; \quad x_2 = \frac{\lambda}{16\pi^2} + \frac{g^2}{4\pi^2} \quad (B.123)$$

$$y_1 = \frac{1}{64\pi^2}(2\lambda M_s^2 \phi_0 - 16gM_f^3) \quad ; \quad y_2 = \frac{1}{64\pi^2}(2\lambda^2 \phi_0^2 + 2\lambda M_s^2 - 48g^2 M_f^2) \quad (B.124)$$

$$\begin{aligned}
z_1 &= m_s^2 \phi_0 + \frac{\lambda}{3!} \phi_0^3 + \frac{\lambda \phi_0 (2 + M_s^2)}{32\pi^2} \left[-\frac{2}{\epsilon} - 1 + \gamma - \log(4\pi/\mu^2) + \psi^{(0)}(\nu + 3/2) + \psi^{(0)}(\nu - 1/2) \right] \\
&\quad - \frac{gM_f(M_f^2 - 1)}{4\pi^2} \left[-\frac{2}{\epsilon} - 1 + \gamma - \log(2\pi/\mu^2) + \psi^{(0)}(M_f + 2) + \psi^{(0)}(M_f - 1) \right] \tag{B.125}
\end{aligned}$$

$$\begin{aligned}
z_2 &= \lambda \phi_0^2 + \frac{\lambda(2 + M_s^2 + \lambda \phi_0^2)}{32\pi^2} \left[-\frac{2}{\epsilon} - 1 + \gamma - \log(4\pi/\mu^2) + \psi^{(0)}(\nu + 3/2) + \psi^{(0)}(\nu - 1/2) \right] \\
&\quad + \frac{\lambda \phi_0 (2 + M_s^2)}{32\pi^2} \left[\psi^{(1)}(\nu + 3/2) + \psi^{(1)}(\nu - 1/2) \right] \left(\frac{\partial \nu}{\partial \phi} \right) \\
&\quad - \frac{g^2(3M_f^2 - 1)}{4\pi^2} \left[-\frac{2}{\epsilon} - 1 + \gamma - \log(2\pi/\mu^2) + \psi^{(0)}(M_f + 2) + \psi^{(0)}(M_f - 1) \right] \\
&\quad - \frac{g^2 M_f (M_f^2 - 1)}{4\pi^2} \left[\psi^{(1)}(M_f + 2) + \psi^{(1)}(M_f - 1) \right] \tag{B.126}
\end{aligned}$$

$x_1, x_2, y_1, y_2, z_1, z_2$ are evaluated at $\phi_{cl} = \phi_0 > 0$.

References

- [1] C. P. Burgess and C. A. Lutken, “Propagators and Effective Potentials in Anti-de Sitter Space,” *Phys. Lett. B* **153** (1985), 137-141 doi:10.1016/0370-2693(85)91415-7
- [2] T. Inami and H. Ooguri, “One Loop Effective Potential in Anti-de Sitter Space,” *Prog. Theor. Phys.* **73** (1985), 1051 doi:10.1143/PTP.73.1051
- [3] T. Inami and H. Ooguri, “NAMBU-GOLDSTONE BOSONS IN CURVED SPACE-TIME,” *Phys. Lett. B* **163** (1985), 101-105 doi:10.1016/0370-2693(85)90201-1
- [4] C. G. Callan, Jr. and F. Wilczek, “INFRARED BEHAVIOR AT NEGATIVE CURVATURE,” *Nucl. Phys. B* **340** (1990), 366-386 doi:10.1016/0550-3213(90)90451-I
- [5] R. Camporesi, “Harmonic analysis and propagators on homogeneous spaces,” *Phys. Rept.* **196** (1990), 1-134 doi:10.1016/0370-1573(90)90120-Q
- [6] R. Camporesi, “Zeta function regularization of one loop effective potentials in anti-de Sitter space-time,” *Phys. Rev. D* **43** (1991), 3958-3965 doi:10.1103/PhysRevD.43.3958
- [7] A. A. Bytsenko, G. Cognola, L. Vanzo and S. Zerbini, “Quantum fields and extended objects in space-times with constant curvature spatial section,” *Phys. Rept.* **266** (1996), 1-126 doi:10.1016/0370-1573(95)00053-4 [arXiv:hep-th/9505061 [hep-th]].

- [8] S. S. Gubser and I. Mitra, “Double trace operators and one loop vacuum energy in AdS / CFT,” *Phys. Rev. D* **67** (2003), 064018 doi:10.1103/PhysRevD.67.064018 [arXiv:hep-th/0210093 [hep-th]].
- [9] O. Aharony, D. Marolf and M. Rangamani, “Conformal field theories in anti-de Sitter space,” *JHEP* **02** (2011), 041 doi:10.1007/JHEP02(2011)041 [arXiv:1011.6144 [hep-th]].
- [10] O. Aharony, M. Berkooz, D. Tong and S. Yankielowicz, “Confinement in Anti-de Sitter Space,” *JHEP* **02** (2013), 076 doi:10.1007/JHEP02(2013)076 [arXiv:1210.5195 [hep-th]].
- [11] M. Kruczenski, J. Penedones and B. C. van Rees, “Snowmass White Paper: S-matrix Bootstrap,” [arXiv:2203.02421 [hep-th]].
- [12] D. Carmi, L. Di Pietro and S. Komatsu, “A Study of Quantum Field Theories in AdS at Finite Coupling,” *JHEP* **01** (2019), 200 doi:10.1007/JHEP01(2019)200 [arXiv:1810.04185 [hep-th]].
- [13] S. Giombi and H. Khanchandani, “CFT in AdS and boundary RG flows,” *JHEP* **11** (2020), 118 doi:10.1007/JHEP11(2020)118 [arXiv:2007.04955 [hep-th]].
- [14] S. Giombi, E. Helfenberger and H. Khanchandani, “Fermions in AdS and Gross-Neveu BCFT,” *JHEP* **07** (2022), 018 doi:10.1007/JHEP07(2022)018 [arXiv:2110.04268 [hep-th]].
- [15] A. Kakkar and S. Sarkar, “On partition functions and phases of scalars in AdS,” *JHEP* **07** (2022), 089 doi:10.1007/JHEP07(2022)089 [arXiv:2201.09043 [hep-th]].
- [16] N. D. Mermin and H. Wagner, “Absence of ferromagnetism or antiferromagnetism in one-dimensional or two-dimensional isotropic Heisenberg models,” *Phys. Rev. Lett.* **17** (1966), 1133-1136 doi:10.1103/PhysRevLett.17.1133.
- [17] S. R. Coleman, “There are no Goldstone bosons in two-dimensions,” *Commun. Math. Phys.* **31** (1973), 259-264 doi:10.1007/BF01646487
- [18] G. W. Gibbons, M. J. Perry and C. N. Pope, “Partition functions, the Bekenstein bound and temperature inversion in anti-de Sitter space and its conformal boundary,” *Phys. Rev. D* **74** (2006), 084009 doi:10.1103/PhysRevD.74.084009 [arXiv:hep-th/0606186 [hep-th]].
- [19] S. Giombi, A. Maloney and X. Yin, “One-loop Partition Functions of 3D Gravity,” *JHEP* **08** (2008), 007 doi:10.1088/1126-6708/2008/08/007 [arXiv:0804.1773 [hep-th]].
- [20] F. Denef, S. A. Hartnoll and S. Sachdev, “Black hole determinants and quasinormal modes,” *Class. Quant. Grav.* **27** (2010), 125001 doi:10.1088/0264-9381/27/12/125001 [arXiv:0908.2657 [hep-th]].

- [21] J. R. David, M. R. Gaberdiel and R. Gopakumar, “The Heat Kernel on AdS(3) and its Applications,” *JHEP* **04** (2010), 125 doi:10.1007/JHEP04(2010)125 [arXiv:0911.5085 [hep-th]].
- [22] R. Gopakumar, R. K. Gupta and S. Lal, “The Heat Kernel on *AdS*,” *JHEP* **11** (2011), 010 doi:10.1007/JHEP11(2011)010 [arXiv:1103.3627 [hep-th]].
- [23] C. Keeler and G. S. Ng, “Partition Functions in Even Dimensional AdS via Quasinormal Mode Methods,” *JHEP* **06** (2014), 099 doi:10.1007/JHEP06(2014)099 [arXiv:1401.7016 [hep-th]].
- [24] V. L. Martin and A. Svesko, “Normal modes in thermal AdS via the Selberg zeta function,” *SciPost Phys.* **9** (2020), 009 doi:10.21468/SciPostPhys.9.1.009 [arXiv:1910.11913 [hep-th]].
- [25] P. Kraus, S. Megas and A. Sivaramakrishnan, “Anomalous dimensions from thermal AdS partition functions,” *JHEP* **10** (2020), 149 doi:10.1007/JHEP10(2020)149 [arXiv:2004.08635 [hep-th]].
- [26] R. Camporesi and A. Higuchi, “On the Eigen functions of the Dirac operator on spheres and real hyperbolic spaces,” *J. Geom. Phys.* **20** (1996), 1-18 doi:10.1016/0393-0440(95)00042-9 [arXiv:gr-qc/9505009 [gr-qc]].
- [27] M. Henningson and K. Sfetsos, “Spinors and the AdS / CFT correspondence,” *Phys. Lett. B* **431** (1998), 63-68 doi:10.1016/S0370-2693(98)00559-0 [arXiv:hep-th/9803251 [hep-th]].
- [28] W. Mueck and K. S. Viswanathan, “Conformal field theory correlators from classical field theory on anti-de Sitter space. 2. Vector and spinor fields,” *Phys. Rev. D* **58** (1998), 106006 doi:10.1103/PhysRevD.58.106006 [arXiv:hep-th/9805145 [hep-th]].
- [29] M. Henneaux, “Boundary terms in the AdS / CFT correspondence for spinor fields,” [arXiv:hep-th/9902137 [hep-th]].
- [30] R. Banach and J. S. Dowker, “Automorphic field theory-some mathematical issues,” *J. Phys. A* **12** (1979), 2527 doi:10.1088/0305-4470/12/12/031
- [31] T. Miyagawa, N. Shiba and T. Takayanagi, “Double-Trace Deformations and Entanglement Entropy in AdS,” *Fortsch. Phys.* **64** (2016), 92-105 doi:10.1002/prop.201500098 [arXiv:1511.07194 [hep-th]].
- [32] S. Sugishita, “Entanglement entropy for free scalar fields in AdS,” *JHEP* **09** (2016), 128 doi:10.1007/JHEP09(2016)128 [arXiv:1608.00305 [hep-th]].
- [33] D. E. Diaz and H. Dorn, “Partition functions and double-trace deformations in AdS/CFT,” *JHEP* **05** (2007), 046 doi:10.1088/1126-6708/2007/05/046 [arXiv:hep-th/0702163 [hep-th]].
- [34] E. J. Weinberg, “Radiative corrections as the origin of spontaneous symmetry breaking,” [arXiv:hep-th/0507214 [hep-th]]

- [35] D. J. Gross and A. Neveu, “Dynamical Symmetry Breaking in Asymptotically Free Field Theories,” *Phys. Rev. D* **10** (1974), 3235 doi:10.1103/PhysRevD.10.3235
- [36] B. Rosenstein, B. Warr and S. H. Park, “Dynamical symmetry breaking in four Fermi interaction models,” *Phys. Rept.* **205** (1991), 59-108 doi:10.1016/0370-1573(91)90129-A
- [37] L. Jacobs, “Critical Behavior in a Class of $O(n)$ Invariant Field Theories in Two-Dimensions,” *Phys. Rev. D* **10** (1974), 3956 doi:10.1103/PhysRevD.10.3956
- [38] B. J. Harrington and A. Yildiz, “Restoration of Dynamically Broken Symmetries at Finite Temperature,” *Phys. Rev. D* **11** (1975), 779 doi:10.1103/PhysRevD.11.779
- [39] U. Wolff, “THE PHASE DIAGRAM OF THE INFINITE N GROSS-NEVEU MODEL AT FINITE TEMPERATURE AND CHEMICAL POTENTIAL,” *Phys. Lett. B* **157** (1985), 303-308 doi:10.1016/0370-2693(85)90671-9
- [40] K. G. Klimenko, “Phase Structure of Generalized Gross-Neveu Models,” *Z. Phys. C* **37** (1988), 457 doi:10.1007/BF01578141
- [41] B. Rosenstein, B. J. Warr and S. H. Park, “Thermodynamics of $(2+1)$ -dimensional Four Fermi Models,” *Phys. Rev. D* **39** (1989), 3088 doi:10.1103/PhysRevD.39.3088
- [42] J. Zinn-Justin, “Four fermion interaction near four-dimensions,” *Nucl. Phys. B* **367** (1991), 105-122 doi:10.1016/0550-3213(91)90043-W
- [43] I.S. Gradshteyn and I.M. Ryzhik, “Table of Integrals, Series, and Products”.